

Review

A Critical Review of Recent Progress and Perspective in Practical Denitration Application

Zhisong Liu ¹, Feng Yu ^{1,2} , Cunhua Ma ¹, Jianming Dan ¹, Jian Luo ³ and Bin Dai ^{1,*}

¹ Key Laboratory for Green Processing of Chemical Engineering of Xinjiang Bingtuan, School of Chemistry and Chemical Engineering, Shihezi University, Shihezi 832003, China; liuzs_shzu@163.com (Z.L.); yufeng05@mails.ucas.ac.cn (F.Y.); mchua@shzu.edu.cn (C.M.); danjmxj@163.com (J.D.)

² Bingtuan Industrial Technology Research Institute, Shihezi University, Shihezi 832003, China

³ Tianjin Key Laboratory for Heavy-Metal Containing Wastewater Treatment, Tianjin 300350, China; qujianluo@hotmail.com

* Correspondence: db_tea@shzu.edu.cn; Tel.: +86-993-205-7272

Received: 19 August 2019; Accepted: 9 September 2019; Published: 13 September 2019



Abstract: Nitrogen oxides (NO_x) represent one of the main sources of haze and pollution of the atmosphere as well as the causes of photochemical smog and acid rain. Furthermore, it poses a serious threat to human health. With the increasing emission of NO_x, it is urgent to control NO_x. According to the different mechanisms of NO_x removal methods, this paper elaborated on the adsorption method represented by activated carbon adsorption, analyzed the oxidation method represented by Fenton oxidation, discussed the reduction method represented by selective catalytic reduction, and summarized the plasma method represented by plasma-modified catalyst to remove NO_x. At the same time, the current research status and existing problems of different NO_x removal technologies were revealed and the future development prospects were forecasted.

Keywords: nitrogen oxide; adsorption De-NO_x; oxidation De-NO_x; selective reduction; nonselective reduction; plasma technology

1. Introduction

NO_x is one of the main sources of haze generation and air pollution in all worldwide. On one hand, NO_x comes from the natural factors of nitrate caused by decay of organism after biological death and plant straw-burning as well as in the lightning process; on the other hand, it stems from the artificial factors, for instance, iron and steel smelting; petroleum cracking and coal-based fossil fuel power generation; fuel vehicle exhaust emissions [1,2]; and NO_x decomposition under the action of soil microorganisms, which is caused by the large amount of nitrogen fertilizer applied in farmland [3,4]. The emission of toxic waste gases has resulted in a significant increase in the content of NO_x in the atmosphere, which is damaging to human organs, such as the heart and lungs, and reducing the body's immunity [5], combining with volatile organic compounds to produce ozone [6], making the human body susceptible to respiratory diseases such as coughs, sore throat, and bronchitis [7,8]; it can also lead to premature birth [9], severely inhibiting photosynthesis, and thus affects plant growth and oxygen conversion [10,11]; but, at the same time, produces photochemical smog [12,13] and acid rain [14]. Furthermore, it forms aerosol with SO₂, dust, and water vapor, then produces PM2.5 and other small particle size air pollution suspensions, namely, haze, which cause serious air pollution worldwide [15,16].

Therefore, the treatment of NO_x is imminent. The supervision of flue gas emission from fixed source factories and the treatment of motor vehicle exhaust emission from mobile sources have been widely controlled [17] recently, appearing to be the following mature technologies; removal of NO_x by

adsorption, oxidation, reduction, and plasma methods. In view of these attentive findings, adsorption method uses recyclable solid adsorbent material to adsorb NO_x from flue gas through microporous structure, remarkably, environmentally friendly, no secondary pollution, and energy-saving and -efficient features make it stand out [18–20]. The oxidation process is a method that oxidizes NO into NO_2 or N_2O_3 with high solubility under the action of an oxidant that is then absorbed by water or alkali solution. The process is simple and cost-saving, and is widely used in the wet flue gas denitrification process with relatively low cost and high removal efficiency of NO_x ; except that the oxidized NO and SO_2 can be removed simultaneously to produce high value-added products [21–23]. The reduction method has the characteristics of high efficiency, cleanliness, and mildness; NO_x removal can be realized at low temperature at present [24–26]. The plasma method is used to modify the surface of the catalyst, the dispersion of active species can be improved by plasma treatment, and the stability and low temperature activity of catalyst can be improved [27,28].

Seldom, if ever, does a comprehensive article to introduce the current situation and treatment methods of removing NO_x . In this paper, we tried to renovate, classify, and summarize the significant perspectives and most relevant findings reported in recent research articles and earlier reviews generalizing the mechanism analysis and research progress of NO_x removal by adsorption, oxidation, reduction, and plasma methods, which can provide means for promoting the technological progress of pollution prevention, maintaining healthy development of factories continuously, studying the methods of removing NO_x deeply, and mastering different technologies of removing NO_x , as well as providing guidance for controlling the emission of NO_x from motor vehicles such as diesel, gasoline, and so on. In order to improve the environmental quality and save the ecological environment, this paper further provides a convenient, low-cost, efficient, and economic guidance line.

2. Removal of NO_x by Adsorption

The adsorption method for NO_x treatment is simple to operate, controllable in process, and can capture toxic waste gases with very low concentration efficiently. NO_x in flue gas is adsorbed by recoverable solid adsorbents through microporous structure [29–31]. The adsorption materials for NO_x in waste gas mainly include molecular sieve, activated carbon, zeolite, heterophony acid, silica gel, and peat [32]. The adsorption method is efficient and thorough, and can produce nitric acid with high added value. Meanwhile, in recent years, adsorption denitrification technology mainly includes the organic framework of copper (Cu-BTC) adsorption and carbon material adsorption methods [33].

2.1. NO_x Removed by Cu-BTC Adsorption

Metal–organic frameworks (MOFs) have many advantages, e.g., porous, high specific surface area, and abundant Lewis acidic active sites, and make excellent gas adsorption materials [34], among them, Cu-based MOFs have excellent catalytic performance [35]. Cu-BTC is a special organic metal framework in MOFs. Qin et al. [36] prepared Agx-Cu-BTC dispersed in bimetallic organic framework by preassembly method to absorb NO_x , this framework had regular octahedral shapes with particle sizes ranging from 10 to 30 microns. Ag-doping into the metal–organic framework of Cu-BTC resulted in a heterojunction, which made the organic functional group, $-\text{COO}-$, blue shift and accompanied with good dispersion of Ag and Cu atoms in the organic framework.

In order to further study the adsorption of NO_x by Cu-BTC material, Khan et al. [37] studied the adsorption of NO in MOFs- $\text{Cu}_3(\text{BTC})_2$ and $\text{Cu}_3(\text{NH}_2\text{BTC})_2$ by ^1H solid-state NMR, and found that ^1H in MOFs- $\text{Cu}_3(\text{BTC})_2$ had a linear relationship with NO adsorption. Kaur et al. [38] explained the synthesis and adsorption properties of Cu-BTC porous octahedral nanocrystals. Meng et al. [39] found that in the framework of Cu-BTC, CO_2 varies with the Langmuir distribution, while the N atom in the NO molecule is mainly responsible for the coordination with the Cu atom. Qin et al. [40] studied the adsorption mechanism of NO on A-Cu-BTC surface (Figure 1a). It was found that the doping of Sr, Ce, Al, and other elements in Cu-BTC could increase the NO conversion (Figure 1b). The modification of Ce by X-ray diffraction analysis enhanced the dispersion of Cu in metal–organic

framework BTC (Figure 1c). Scanning electron microscopy further confirmed that the formation of Ce–Cu heterojunction enhanced the low degree (Figure 1d).

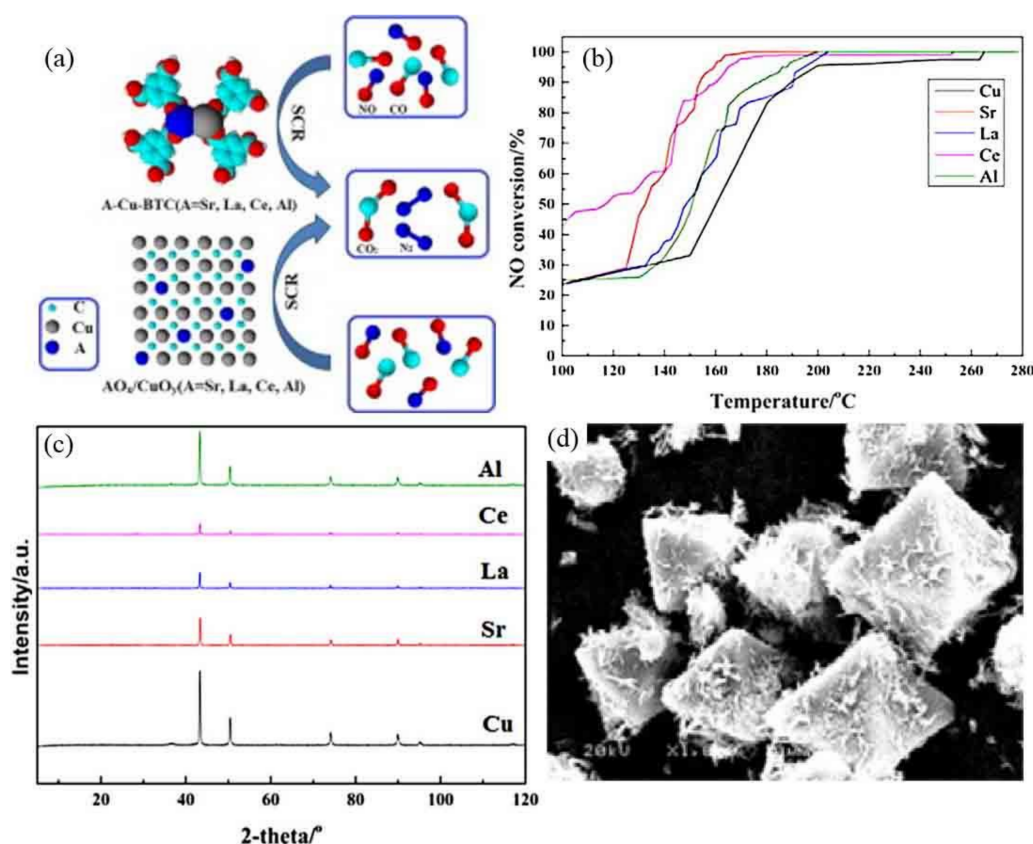


Figure 1. (a) Adsorption process and reaction mechanism of NO on A-Cu-BTC, (b) NO conversion with different metal dropping, (c) XRD images of metal doped Cu-BTC, and (d) SEM images of A-Cu-BTC [40]. Reproduced with the permission from Ref. [40], Copyright 2016, Elsevier.

2.2. NO_x Removed by Carbonaceous Material Adsorption

Removal of NO_x by adsorption, especially activated carbon, has undergone a long historical evolution [41]; activated carbon originated from 1900, and its inventor was Raphael von Ostrejko, by whom, British and German patents had been obtained. In 1920, the demand for activated carbon continued to expand through the extensive application of gas masks; at the same time, the application of activated carbon in sewage treatment and catalysis was gradually developed [42,43], activated carbon plants in major industrial countries, including the United States, had been gradually opened and expanded. In the mid-20th century, the field of activated carbon continued to aggrandize and was regarded as “universal adsorbent”. Today, activated carbon is used in pollution control [44,45] with a high-precision instrument to produce pore structure matching the molecular size of the toxic waste gas, which is used to adsorb harmful gases such as benzene, formaldehyde, NO_x, NH₃, and so on [46,47].

Activated carbon, which is not a natural material, but an artificial material made by processing carbon-containing organic matter, has been widely used as catalyst [48]. Activated carbon comes from a wide range of raw materials, which can be almost any organic compound material, including sawdust, bagasse, branches, shells and other wood materials [49], coking coal, bituminous coal, and other bulk commodities [50]. In the process of activation smelting, a huge specific surface area and complex pore structure are gradually formed, which can effectively remove chroma and odor, and remove most organic pollutants and some inorganic substances in secondary effluent [51], containing some toxic heavy metals [52,53]. Furthermore, activated carbon has excellent thermal and chemical

stability, high wear resistance and a variety of oxygen-containing functional groups on the surface, so activated carbon adsorption is a very promising means in the process of flue gas treatment.

Different kinds of oxygen-containing groups are the main active sites on activated carbon [54]; however, the untreated activated carbon has smaller pore volume and specific surface area, higher ash content, and poor adsorption performance. The chemical properties of activated carbon surface can be changed by chemical oxidation, reduction, and loading [55,56]. Jie et al. [57] found that proper oxidation could improve the degradation ability of activated carbon to nitrogen compounds. Wang et al. [21] found that pretreatment of carrier activated carbon with HNO_3 could improve the NO conversion. Li et al. [58] discovered that the pore size of activated carbon fibers decreased and the surface functional groups increased after modification with $\text{Cu}_2\text{O}/\text{TiO}_2$, which improved the adsorption capacity of activated carbon fibers for NO. Javier et al. [59] prepared goethite and hematite twin grains on activated carbon, which improved the total denitrification capacity. You et al. [60] caused defects on the surface of activated carbon by changing pore size and nitrogen doping, which greatly improved its NO catalytic oxidation activity at room temperature. Sun et al. [61] used Cu-Fe modified microwave coconut shell activated carbon (CuFe/MCSAC) to remove NO from industrial tail gas, and studied the adsorption process of NO on the surface of activated carbon (Figure 2a). It was found that 3% O_2 was beneficial to increase the conversion of NO, which was attributed to NO oxidation as the first step of selective catalytic reduction reaction (Figure 2b). In addition, the sulfur resistance was studied (Figure 2c,d). The preparation methods and other conditions of different adsorption materials are shown in Table 1.

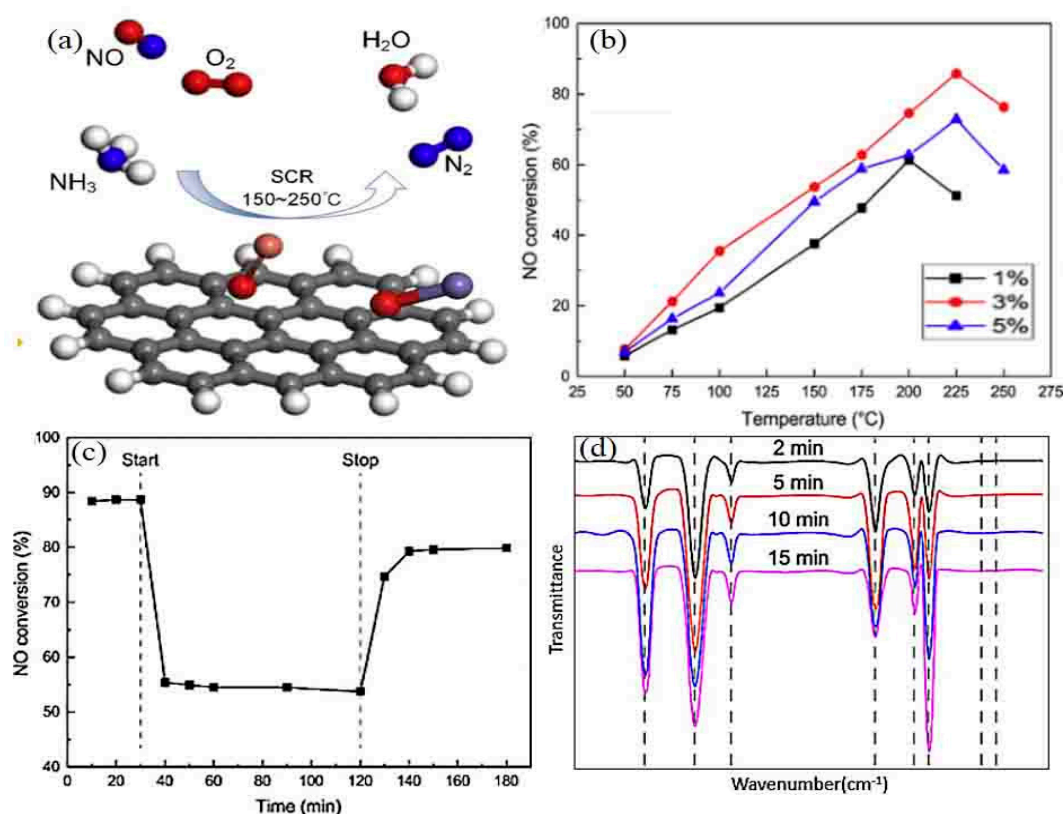


Figure 2. (a) Adsorption process of NO on activated carbon surface, (b) effect of adding O_2 on NO conversion, (c) study on SO_2 resistance of Cu-Fe/MCSAC catalyst, and (d) in situ infrared analysis of Cu-Fe/MCSAC after SO_2 entering gas pool [61]. Reproduced from Ref. [61], Copyright 2019, Elsevier.

Table 1. Effect of different adsorption materials on NO conversion.

Adsorbent Material	Synthetic Method	Reaction Conditions	Temperature (°C)	Conversion (%)	Ref.
Ag-Cu-BTC	preassembled method	500 ppm NO, GHSV 10,000 h ⁻¹ , N ₂	238	100	[36]
Zeolite	Wetness impregnation	250 mg/m NO, 1000 mg m ⁻³ SO ₂ GHSV 150 L h ⁻¹ , N ₂	250	91.7	[62]
Gas-phase	microwave	600 ppm NH ₃ , 3% O ₂ , and GHSV 30,000 h ⁻¹ N ₂	80	50	[61]
ACF	Precipitation method	Flue gas 0.1–1%, GHSV 1000 mL/min, N ₂	40	60	[58]
AC	Nitric acid hydrothermal	1000 ppm NO, 20 vol.% O ₂ GHSV 16,000 h ⁻¹ N ₂	25	56.6	[60]

2.3. Other Crucial NO_x Adsorbents

There are numerous kinds of NO_x adsorbents; low-priced and efficient adsorbents are required for denitrification. Li et al. [63] prepared fly ash derivative Cu/SAPO-34 by acid–alkali combined hydrothermal method to absorb NO_x. Mire et al. [64] studied the removal of NO_x using H-ZSM-5 as adsorbents, and found that Fe-modified Fe/H-ZSM-5 had the strongest adsorption capacity. Chen et al. [65] synthesized Fe-ZSM-5@CeO₂ adsorbent for adsorbing NO_x. Baran et al. [66] prepared Cu-BEA molecular sieve to study the adsorption characteristics of NO_x. Ma et al. [67] developed a new Ag nano-g-C₃N₄/WS₂ material to adsorb NO_x. Imai et al. [68] developed a niobium phosphate adsorbent to remove NO_x. Xiao et al. [69] studied the adsorption of NO_x on mesoporous molecular sieve doped with platinum (Pt/SBA-15). Wang et al. [70] found that when iron and cobalt were loaded on the active semi-coke material; it was beneficial to NO_x adsorption. Chen et al. [71] studied NO removal performance based on sinter adsorption materials. The synthetic methods and reaction conditions of different adsorption materials are shown in Table 2.

Table 2. Effect of different adsorbents on removal of NO_x.

Adsorbent Material	Synthetic Method	Reaction Conditions	NO Conversion %	Ref.
Cu/SAPO-34	Acid–alkali hydrothermal	300 ppm NO, 3% O ₂ GHSV 12,000 h ⁻¹ , N ₂	90	[63]
Fe/H-ZSM-5	Hydrothermal	5000 ppm NO, 5% O ₂ , GHSV = 35,000 h ⁻¹ , He	63.4	[64]
Fe-ZSM-5 @CeO ₂	Dopamine polymerization	1000 ppm NO, 5% O ₂ , GHSV 33,600 h ⁻¹ , N ₂	90	[65]
Cu-BEA	Precipitation	1000 ppm NO, 3.5 vol% O ₂ 1000 mL/min, N ₂	100	[66]
g-C ₃ N ₄ /WS ₂	Solvent evaporation	500 ppm NO, 20 vol% O ₂ , GHSV 400 mL/min, N ₂	72.5	[67]
Niobium phosphate	Impregnation	1000 ppm NO, 1125 ppm O ₂ , GHSV 100 mL/min, He	100	[68]
Pt/SBA-15	Thermal hydrolysis	4000 ppm NO, 10 vol% O ₂ , GHSV 50 mL/min, Ar	100	[69]
Semi-coke	Hydrothermal	1000 ppm NO, GHSV 6000 h ⁻¹ , N ₂	100	[70]
Sintered ore	Impregnation	400 mg/m ³ NO, 15% O ₂ , GHSV = 1000 h ⁻¹ , Ar	61.6	[71]

Chemical adsorption usually requires a certain activation energy, and the adsorption rate is slow at low temperature [72]. The adsorption method is closely related to the surface chemical properties of adsorbents, and it can not only eliminate the pollution of NO_x to the atmosphere, but recycle them to produce high value-added products. However, due to its limited adsorption capacity, the size of the absorber is huge, the adsorbent needs to be regenerated frequently, and the one-time investment is large. In particular, activated carbon has the possibility of spontaneous combustion above $300\text{ }^\circ\text{C}$, which causes considerable difficulties in the regeneration of adsorbents and limits its application.

3. Removal of NO_x by Oxidation

Since MeKee oxidized low-concentration NO to NO_2 in 1921; it laid the foundation for NO oxidation [73]. In the early 1980s, Japanese scholars made a more in-depth study on the oxidative denitrification. At this time, NO oxidative denitrification technology rose gradually. In the late 1990s, Takashi Ibusuki et al. [74] found that TiO_2 can oxidize NO to HNO_3 under ultraviolet irradiation rapidly. Nowadays, the technology of removing NO_x by oxidation is relatively mature. It can not only control the morphology of catalysts by some means, but study the law that affects the activity of catalysts. At the same time, investigators often only study the activity of catalysts in a low-temperature window gradually [75–77]. This method uses oxidizer to oxidize NO, which is not soluble in water, to NO_2 or N_2O_3 in flue gas [78–80], which is then sprayed and washed by water, alkali solution, acid solution, or metal complex solution so that the NO_x in the gas phase are transferred to the liquid phase to realize the denitrification treatment of the flue gas. O_3 , ClO_2 , NaClO_2 , NaClO , KMnO_4 , H_2O_2 , Cl_2 , and HNO_3 can be used as oxidants [81]. According to the types of oxidation technology, it can be divided into gas-phase oxidation, liquid-phase oxidation, and catalytic oxidation.

3.1. NO_x Removed by Gas-Phase oxidation

Since the development of a low temperature oxidation technology called LoTO_x by Linde Industrial Gases Company in the United States, more and more researchers have been studying the denitrification performance of O_3 . The gas-phase oxidation method has been used to purify flue gas from boilers fueled with natural gas, and the denitrification rate is over 90%. The purification process is simple and has no effect on the normal operation of the boiler. It can recover high-grade HNO_3 [82,83]. O_3 is highly oxidizable, and the reduction potential in the process of $\text{O}_3 \leftrightarrow \text{O}_2$ can reach 2.07 eV, which makes the oxidation of NO possible.

At present, ClO_2 and O_3 are widely used in oxidative denitrification as gas phase oxidants. Hultén et al. [84] found that when the molar ratio of ClO_2 to NO was 0.6 at $160\text{ }^\circ\text{C}$, the total amount of NO_x removed was 94%. Sun et al. [85] discovered that the removal efficiency of NO_x increased with increasing O_3 concentration. The removal efficiency of NO_x reached 82% when the flue gas temperature exceeded $40\text{ }^\circ\text{C}$. Mok et al. [86] proposed a two-step process consisting of an O_3 chamber and an absorber containing a reductant solution for simultaneous removal of NO_x . When the flue gas passes through the O_3 chamber, and in turn the absorber, the removal rate of NO_x is ~95%. Lin et al. [87] studied the deep oxidation of NO by O_3 on the MnO_x -based catalyst. The experimental device of deep oxidation showed that the catalyst had good stability and sulfur resistance. Han et al. [88] prepared the black TiO_2 catalyst by sol-gel method. The deep oxidation of NO to HNO_3 was further strengthened (Figure 3a): black TiO_2 had higher NO conversion than TiO_2 at the low temperature of $60\text{ }^\circ\text{C}$ (Figure 3b). New peaks of black TiO_2 at 532.6 eV were found by X-ray photoelectron spectroscopy (XPS) chromatography, which further confirmed the excellent catalytic activity of black TiO_2 (Figure 3c). In addition, the sulfur resistance of black TiO_2 was investigated (Figure 3d).

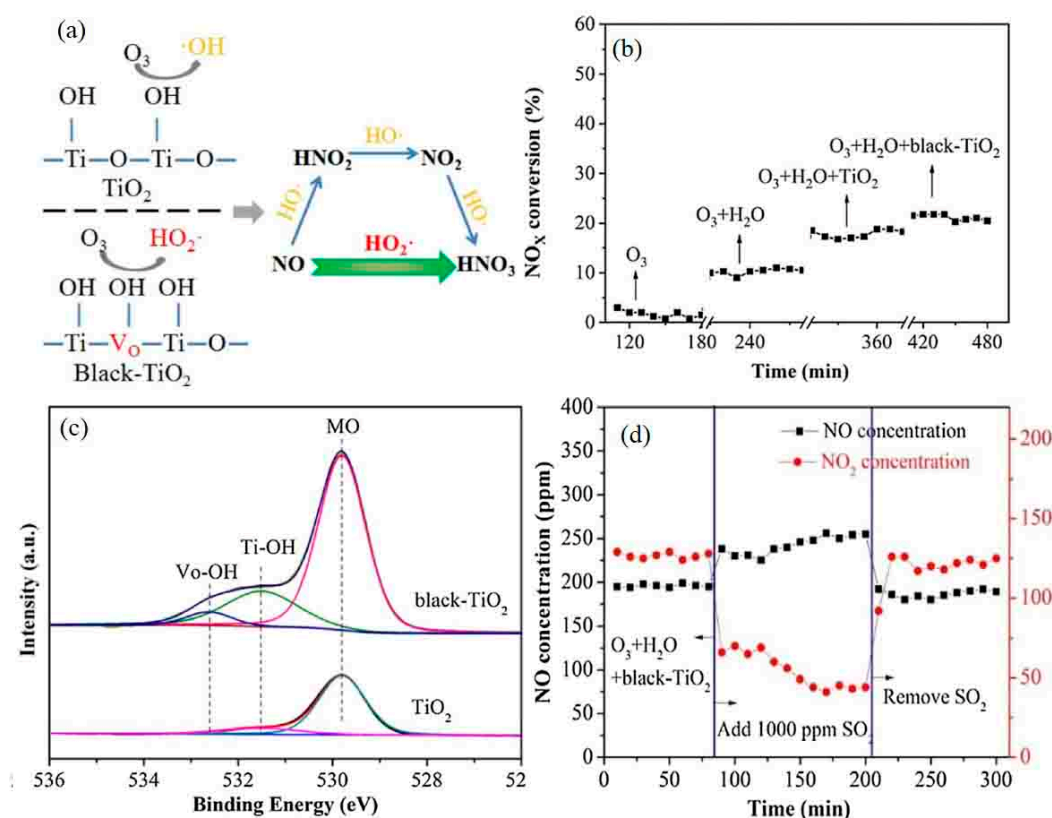


Figure 3. (a) Reaction mechanism of NO_x removal by O₃ in black TiO₂, (b) de-NO_x performance at 60 °C, (c) X-ray photoelectron spectroscopy (XPS) analysis under different conditions, and (d) sulfur resistance of black TiO₂ under 1000 ppm SO₂ [88]. Reproduced from Ref. [88], Copyright 2018, Elsevier.

3.2. NO_x Removed by Liquid-Phase Oxidation

The liquid-phase oxidation absorption method is that NO is oxidized by liquid phase oxidant and then absorbed by alkali absorption method. The de-NO_x rate can reach 90–95% when using KMnO₄ or NaClO₂ as liquid phase oxidizers [89]. NaClO₂ has strong oxidizing property; its solution can oxidize NO to NO₂, and then NaNO₃ was obtained. It is easy to oxidize NO with NaClO₂ and the removal rate of NO is high [90]. In order to cope with the increasingly severe environmental problems and find effective ways to control air pollution, the NO gas discharged from flue gas can be removed simultaneously through a wet NaClO₂ scrubber combined with a plasma electrostatic precipitator.

Deshwal et al. [91] used NaClO₂ solution to remove NO_x from simulated flue gas. NaClO₂ was a better oxidant when the pH was less than 4. NaClO₂ was decomposed into ClO₂ gas in acidic medium. It was considered that NaClO₂ participates not only in NO oxidation but in NO₂ absorption. Hao et al. [92] prepared a new composite oxidant NaClO₂/Na₂S₂O₈, removing SO₂ and NO simultaneously by pre-oxidation. The removal rates of SO₂ and NO were 100% and 82.7%, respectively, under the optimum conditions. Yang et al. [93] used ultraviolet radiation sodium chlorite (UV/NaClO₂) solution to remove NO_x from simulated flue gas in a small scrubbing reactor. The results showed that the addition of Cu and Mn resulted in the lattice expansion and micro-strain decrease of CeO₂-ZrO₂, which led to the formation of oxygen vacancies. Besides, there was a strong interaction between surface Cu, Mn, and Ce through charge transfer.

3.3. NO_x Removed by Catalytic Oxidation

O_3 has a high preparation cost in gas-phase oxidation, which leads to its narrow promotion area; the liquid-phase oxidation method requires higher corrosion resistance of equipment, and the price of oxidant is relatively expensive, which restricts its industrial application. Therefore, the preponderance of catalytic oxidation method are beginning to highlight [94]. The oxidant is the excess oxygen in flue gas, the catalysts are vanadium, tungsten, and titanium and rare earth metal oxides supported on activated carbon, alumina, and silica. This method has been widely used in flue gas purification with the denitrification rate is over 90% [95]. The preponderance of catalytic oxidation are closed-circuit circulation; simultaneous removal of SO_2 , dust, and other pollutants without additional oxidizer; injection of 5% steam into flue gas can improve the efficiency and life of catalyst; and low investment and operation cost of equipment. Catalytic oxidation technology for NO_x removal includes molecular sieve catalytic oxidation, metal oxide catalytic oxidation and Fenton system catalytic oxidation, which have their respective applicable conditions.

3.3.1. Catalytic Oxidation of Molecular Sieve

A kind of natural aluminosilicate, which has the functions of ion exchange, molecular sieving, catalysis and adsorption, called zeolite, and synthetic zeolite is also called molecular sieve. The basic structure of molecular sieve skeleton is Al_2O_3 and SiO_4 tetrahedrons, which form a three-dimensional network structure by combining the common O atoms [96]. It has strong selectivity, high-temperature resistance, and high adsorption capacity, which is widely used in organic chemical industry and petrochemical industry. It is also an excellent adsorbent for gas dehydration. At the same time, more and more attention has been paid to the purification of waste gas. Molecular sieves have regular and uniform intracrystalline channels, and the pore size is close to the molecular size. The catalytic performance of molecular sieves varies significantly with the geometrical size of reactant molecules, product molecules or reaction intermediates [97].

Molecular sieve catalysts for NO treatment are mostly used in oxidation and decomposition processes, such as octahedral molecular sieve (OMS-2) catalysts. Molecular sieve catalysts for oxidation reaction are mainly transition metal ion exchange zeolites and specific types of zeolite zeolites, and these zeolite catalysts only show high temperature activity. Liu et al. [98] first used solvent-free synthesis of cryptomelane OMS-2 to oxidize waste material in coal-fired flue gas, which provided a new idea for oxidative denitrification by molecular sieve. Geng et al. [99] prepared zinc oxide nanoparticle molecular sieves by melt infiltration method to remove exhaust gas at room temperature. Saminda et al. [100] synthesized Mn octahedral molecular sieve (OMS-2) to remove flue gas by catalytic oxidation. Park et al. [101] studied the equilibrium and kinetics of adsorption of N_2O on carbon molecular sieves, concluding that the adsorption rate of N_2O was influenced by kinetics and Lewis structure. Sarmah et al. [102] analyzed the microstructure and morphology of OMS by scanning electron microscopy, which showed the highly cross-linked nanowire morphology. Hamaguchi et al. [103] studied the mechanism of NO removal on the surface of molecular sieve $\text{K}_{1.14}\text{Mn}_8\text{O}_{16}$ (Figure 4a), finding that the thermal unstable oxygen potential acted as the oxidation site of NO at low temperature. The doping of K increased the adsorption of NO (Figure 4b). The particle size of K was 0.46 nanometers (Figure 4c). NO generated in K-OMS-2 molecular sieves NO_3^- , the formation of NO_3^- is proved by Kubelka–Mung theory (Figure 4d).

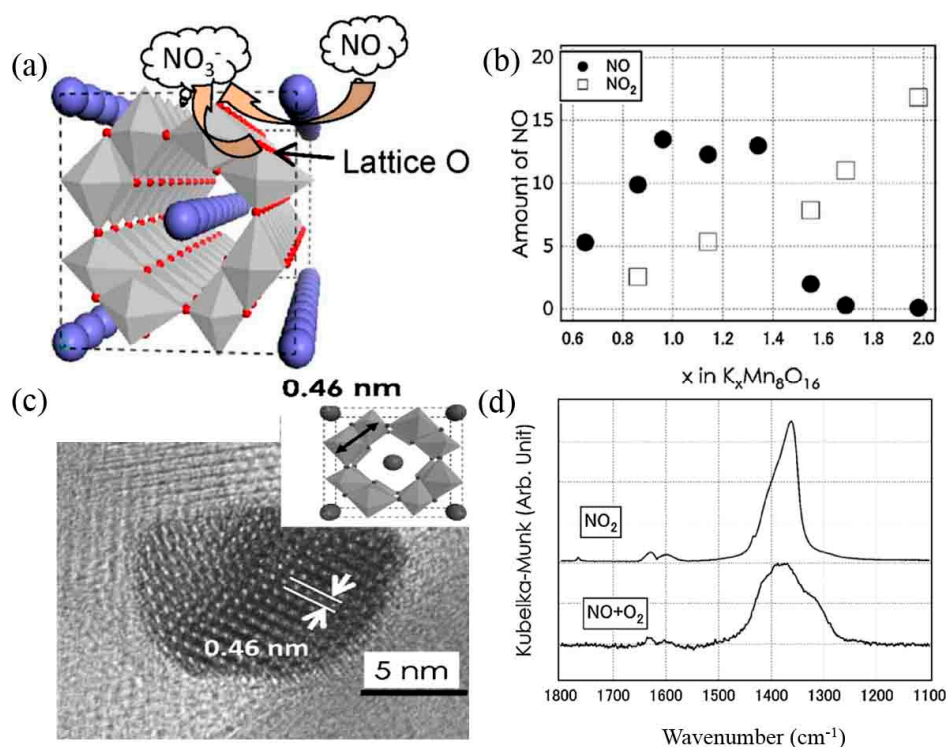


Figure 4. (a) Reaction mechanism of NO oxidation on OMS-2, (b) concentration changes of NO and NO₂ with K-doping, (c) morphology of OMS-2, and (d) Kubelka–Mung function diagram [103]. Reproduced from Ref. [103], Copyright 2016, Elsevier.

3.3.2. Catalytic Oxidation of Metal Oxides

Metal oxide, the compound of O and another metal element, is a kind of excellent catalyst. As the main catalyst, promoter and carrier, it has been widely used in the field of catalysis. After nanotreatment of metal oxides, nano-materials with uniform dispersion, small particle size, and high purity can be obtained, and their catalytic performance is better [104]. Metal oxides provide oxygen free radical formation products for reactants and provide active sites for adsorption (or coordination) of reactants to make them active as well.

Metal oxide is a kind of catalyst that has been studied earlier in the field of NO catalytic oxidation and developed vigorously. Jogi et al. [105] found that the presence of TiO₂ greatly enhanced the efficiency of O₃ oxidation of NO₂ to N₂O₅ at 100 °C. Wang et al. [106] synthesized manganese oxides with different valences (MnO₂, Mn₂O₃, and Mn₃O₄) by hydrothermal method. At the space velocity of 48,000 mLg⁻¹h⁻¹, with oxygen as oxidant, the maximum NO conversion rate was 91.4%. Ma et al. [107] synthesized nanoparticle-like monocrystalline SmMn₂O₅ by adjustable hydrothermal method; among them, nanoparticle-like SmMn₂O₅ achieved more than 90% NO conversion at 300 °C. Jia et al. [79] synthesized a series of Mn–Fe catalysts for oxidative denitrification by hydrothermal method. It was found that the addition of iron oxides could effectively improve the catalytic oxidation performance of manganese dioxide at low temperature. Cai et al. [108] synthesized Cr–Ce oxidative denitrification catalyst with three-dimensional structure by hydrothermal method; more active sites could be exposed with the increase of surface particle size and roughness (Figure 5a). The chromium-Ce/Et catalyst synthesized with ethanol as solvent had the highest catalytic oxidative denitrification activity (Figure 5b). Through a series of characterization catalysts, the Cr–Ce/Et coexistence effect formed the phase interface between atoms (Figure 5c). In addition, the effects of steam and SO₂ on NO conversion over Cr–Ce/Et catalysts at 250 and 300 °C were studied (Figure 5d).

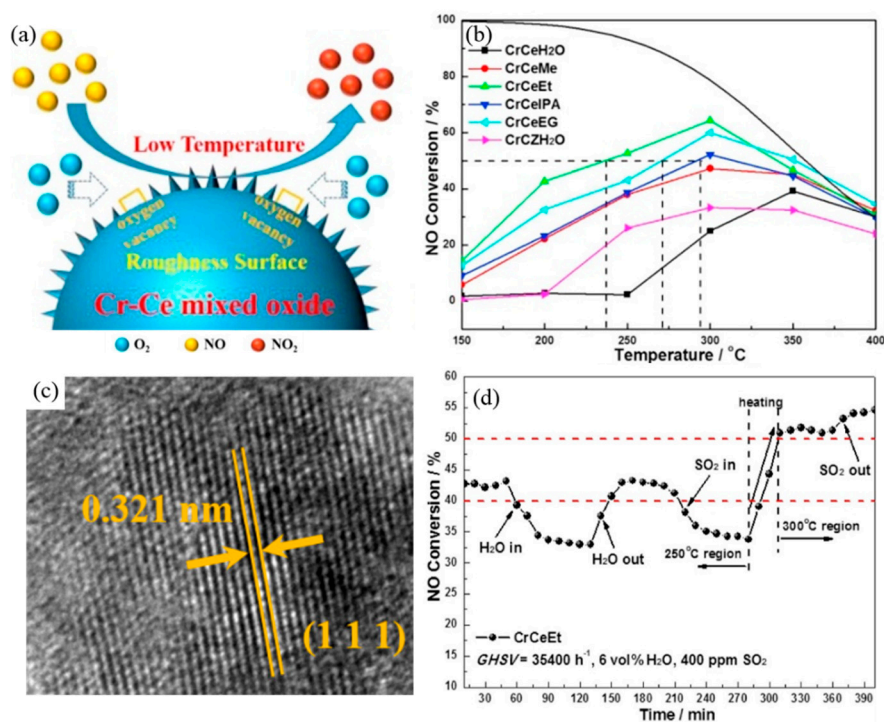


Figure 5. (a) Surface oxidation mechanism of 3D spherical Cr–Ce mixed oxides, (b) NO conversion of hydrothermal synthesis catalysts with different solvents, (c) HRTEM image of Cr–Ce/Et catalysts, and (d) sulfur and water resistance at 250–300 °C [108]. Reproduced from Ref. [108], Copyright 2018, Elsevier.

3.3.3. Photocatalytic Oxidation

Photocatalytic oxidation is a new process of NO_x treatment, which has been developed gradually over the last ten years. The principle of photocatalytic oxidation is to irradiate semiconductor catalysts with light of specific wavelength, to stimulate valence band electrons on semiconductor materials to transit into conduction band, and to generate holes in valence band. Conduction band electrons and valence band holes have strong reductive and oxidative properties, respectively. When they are in contact with flue gas, H₂O, O₂, and NO_x adsorbed on the catalyst surface will generate active free radicals under the action of light, and then catalytic oxidation reaction will take place to oxidize NO_x to NO₃⁻. Because it does not need to inject additional reductant and is simple to operate with low-cost and no secondary pollution, it is the focus of photocatalytic technology research at present [109,110].

The catalysts for photocatalytic oxidation are mainly metal oxide semiconductor materials. Among them, TiO₂ has the merits of high catalytic activity, photochemical stability and low price. It is the most commonly used catalytic material in photocatalytic reaction. Duan et al. [111] found that a small amount of Ag nanoclusters supported on TiO₂ was beneficial to improve photocatalytic activity. He et al. [112] synthesized carbon-encapsulated nanocrystalline TiO₂ catalyst, which achieved 71% NO conversion under visible light. Yuan et al. [113] prepared TiO₂ aluminosilicate fiber nanocatalyst for photocatalytic removal of NO_x. Jin et al. [114] prepared SrTiO₃ catalyst with SrCO₃ successfully as auxiliary by one-step in situ pyrolysis for removal of NO_x. Huy et al. [115] reported for the first time the removal of NO_x by visible light on SnO₂/TiO₂ nanotube heterojunction catalysts. The reaction mechanism was shown in Figure 6a. The removal efficiency of NO_x under visible light was represented in Figure 6b. Figure 6c shows that SnO₂/TiO₂ nanotube heterojunctions had been successfully synthesized. Figure 6d proves that the superoxide anion radical played an important role in visible light photocatalytic oxidation by using active oxygen detection materials.

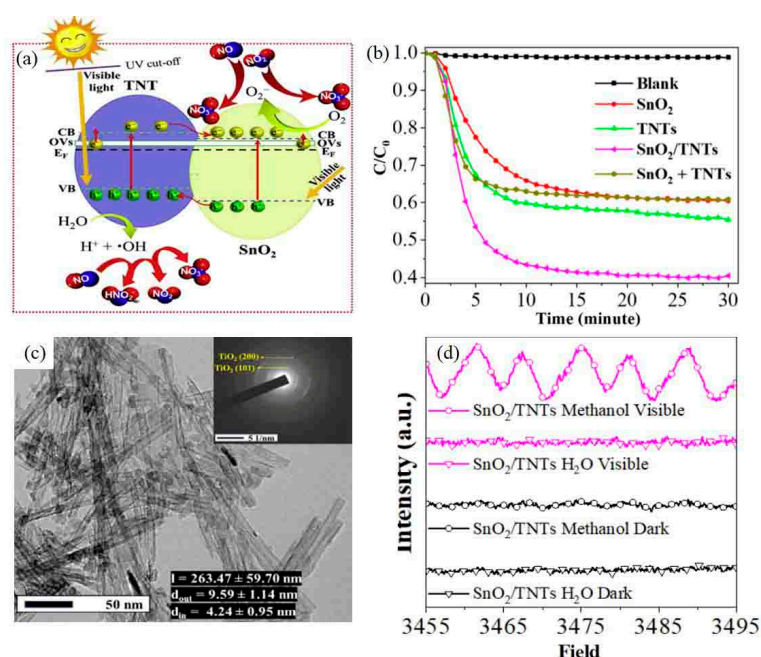


Figure 6. (a) Reaction mechanism of visible light removal of NO_x by SnO₂/TiO₂ nanotube heterojunction, (b) removal efficiency of NO_x under different conditions, (c) transmission electron microscopy of SnO₂/TiO₂ nanomaterials, and (d) detection process of free radicals under different conditions [115]. Reproduced from Ref. [115], Copyright 2019, Elsevier.

3.3.4. Catalytic Oxidation of Fenton System

The essence of Fenton system is that the chain reaction between Fe²⁺ and H₂O₂ catalyzes the production of OH· with strong catalytic oxidation ability. Its oxidation potential is only 2.80 V after that of fluorine, which is a strong oxidation system. In addition, OH· has high electrophilicity and electronegativity and its electron affinity can reach 569.3 kJ, which is associated with strong additive reaction properties. Therefore, Fenton reagent can selectively degrade most organic compounds in water, especially suitable for the treatment of organic wastewater which is difficult to be degraded by biology or chemical oxidation. The prospect of catalytic oxidation of NO_x in flue gas is also extremely promising [116,117].

NO can be oxidized efficiently at low temperature with H₂O₂. At present, Fenton reagents and Fenton-like reagents are widely studied [118,119]. H₂O₂, no secondary pollution and low price, is one of the main components of Fenton reagent and can achieve high denitrification rate [120]. Fenton reagent refers to the H₂O₂/Fe²⁺ system, through a series of catalytic actions of Fe²⁺ to produce iso-strong oxides OH·, HO₂·, and O₂⁻. Wang et al. [121] adopted a new Fenton process catalyzed by Cu²⁺ and Fe²⁺ in coordination, which inducing more OH· to deoxidize NO, and enhancing the denitrification activity of Fenton catalyst. Zhao et al. [122] carried out simultaneous denitrification of flue gas in bubbling reactor with Fenton reagent. The removal rate of NO was over 90%. Cheng et al. [123] found that too high Fe²⁺ concentration and pH were not conducive to NO oxidation and when the pH was only 2–5, the formation rate of OH· reached the maximum. Guo et al. [124] confirmed that the oxidation of NO by Fenton reagent occurred on the liquid membrane side, low concentration of NO was not conducive to mass transfer to the liquid side. Cui et al. [125] took fly ash as raw material and removed NO_x with hydrogen peroxide. It is found that Fenton heterogeneous catalyst modified by alkali, acid, and alkali has high catalytic activity. Zhao et al. [126] used heterogeneous ultraviolet spectrophotometry to remove SO₂ and NO from flue gas for the first time. Yuan et al. [127] oxidized NO with H₂O₂ as oxidant in the two-ion Fenton reaction system (Figure 7a,b). The modification of Ce could significantly improve the conversion of NO (Figure 7c). The effect of Ce on the dispersion of Fe²⁺ was further investigated by XRD (Figure 7d).

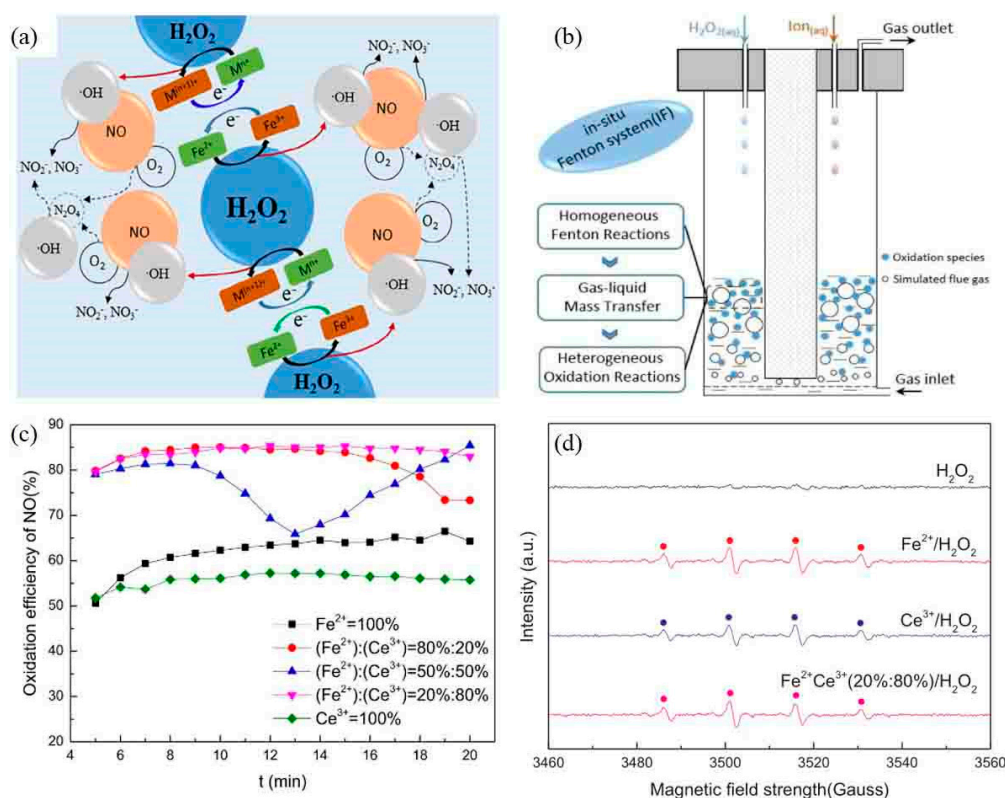


Figure 7. (a) Reaction mechanism of in situ Fenton system with two-ion reagents, (b) schematic diagram of in situ Fenton system, (c) effect of Ce-doping with different proportion on NO conversion, and (d) XRD was used to further explore the effect of Ce on the dispersion of Fe²⁺ [127]. Reproduced from Ref. [127], Copyright 2018, Elsevier.

In recent years, oxidation method has been widely used in the United States and European countries to remove NO_x. Selective catalytic oxidation method has the advantages of relatively low cost and high removal efficiency of NO_x. The oxidized NO can be removed simultaneously with SO₂ to produce high value-added products. The process is simple and cost-saving [128,129]. The reagents materials and other conditions of different oxidation methods are shown in Table 3.

Table 3. Removal of NO_x by oxidation.

Oxidation Method	Reagents Materials	Temperature (°C)	NO Conversion (%)	Reference
Gas phase	ClO ₂	160	94	[84]
	O ₃	40	82	[85]
	O ₃	60	95	[88]
Liquid phase	UV/NaClO ₂	50	98.1	[92]
	NaClO/NaClO ₂	50	85	[90]
	NaClO ₂ /Na ₂ S ₂ O ₈	120	82.7	[92]
Catalytic oxidation	K-OMS-2	50	-	[103]
	MnO _x	250	91.4	[106]
	SmMn ₂ O ₅	300	90	[107]
	Fe _{0.32} MnO ₂	250	80	[79]
	Fenton	140	90	[125]
	La _{0.8} Pr _{0.2} MnO ₃	260	91	[130]

4. Removal of NO_x by Reduction

As early as the late 1970s, reduction denitrification technology was put into use in Japan. Over time, reduction technology had been widely used in Europe and the United States, and is considered to be the most advantageous technology for removing NO_x. Because of the limitations of NO_x control before and during combustion, the control of NO_x in flue gas after combustion has attracted wide attention [131]. There are many technologies for removing NO_x from flue gas, according to different principles, they can be divided into catalytic reduction and adsorption, besides, in the view of different working media, and they can be divided into dry and wet methods. Different treatment methods are selected according to the concentration of NO_x tail gas and other working conditions [132–134]. Reduction denitrification technology includes selective noncatalytic reduction and selective catalytic reduction.

4.1. Selective Noncatalytic Reduction (SNCR) for NO_x Removal

Selective noncatalytic reduction (SNCR) has been developed earlier and its technology is relatively mature, which can generally reduce NO_x by 50 to 60%. The main principle is that under the condition of catalyst, ammonia, or urea with reductive groups are injected into the flue gas of high temperature furnace was between 850 and 1100 °C. NO_x in the flue gas is reduced to harmless nitrogen after atomizing and spraying into the reactor. The advantage of SNCR technology is that there is less investment and occupied area a relatively small, SNCR technology has certain limitations and is generally only suitable for small coal-fired boilers with low NO_x content [135]. Since there is no catalyst to accelerate the reaction, the operating temperature is higher than that of SCR method. In order to avoid NH₃ being oxidized, the temperature should not be too high. The current trend is to use urea instead of NH₃ as reducing agent.

In order to further study the development status of selective noncatalytic reduction (SNCR), Hao et al. [136] found that in the process of SNCR containing NH₃, the use of water vapor could increase NO reduction rate, and the optimum water vapor content was 4–8%. Sodium and potassium additives could promote NO reduction in the order of Na₂CO₃ > KCl > NaCl. Fu et al. [137] found that CaO had an effect on the pyrolysis of urea during melt coalescence, thus reduced the pyrolysis rate of urea and the performance of urea SNCR denitrification process. Chen et al. [138] found that when urea was added into hydrazine hydrate solution, better denitrification efficiency could be obtained in the temperature range of 550 to 650 °C. Kang et al. [139] validated the optimized SNCR reaction mechanism, and combined the optimized mechanism with CFD software to simulate the SNCR denitrification process. Fu et al. [140,141] studied the reaction mechanism of SNCR denitrification on CaO and CaCO₃ surfaces (Figure 8a). NH₃ conversion and NO selectivity in different mixed gas without oxygen were analyzed (Figure 8b), HCHO was the main product of NH₃ transformation on CaCO₃ surface (Figure 8c), and in situ infrared spectroscopy further confirmed the species of reaction intermediates (Figure 8d).

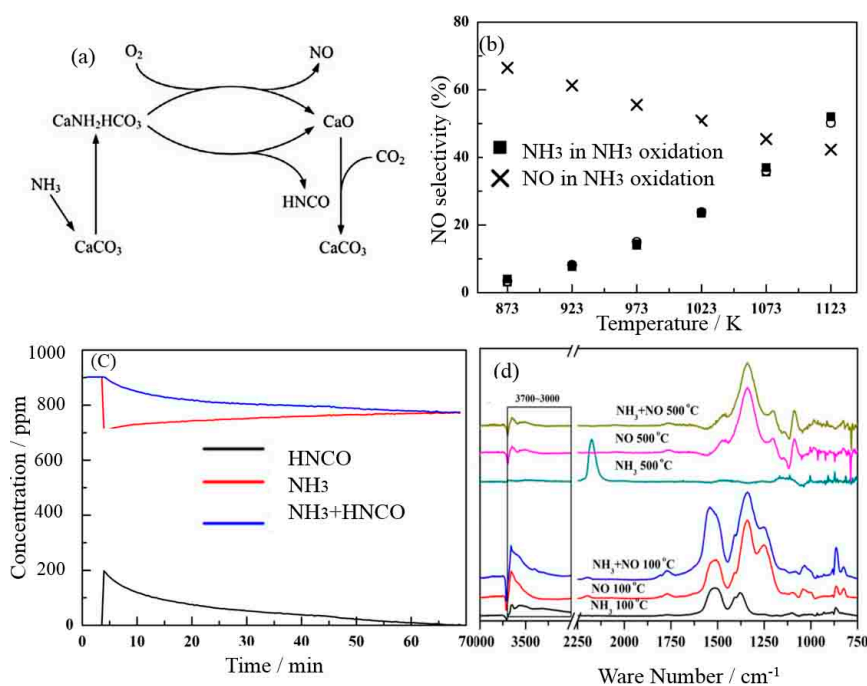


Figure 8. (a) Reaction mechanism of selective noncatalytic reduction (SNCR) on CaCO₃ surface, (b) NH₃ conversion and NO selectivity in different mixed gas, (c) FTIR analysis of CaCO₃ surface active species, and (d) in situ FTIR analysis of reaction intermediates at 500 °C [140,141]. Reproduced from Ref. [140], Copyright 2016, Elsevier; Reproduced from Ref. [141], Copyright 2015, Elsevier.

4.2. Selective Catalytic Reduction (SCR) for NO_x Removal

SCR is one of the most widely used denitrification methods at home and abroad at present. It was first developed by the United States, and then widely used in industrial production in Japan. SCR can make the removal efficiency of NO_x reach more than 90% [142,143]. The basic principle of SCR technology is that under the existence of catalyst, NH₃, CO, and other reducing agents are used to reduce the NO_x to N₂ in flue gas. At the same time, this method also has some shortcomings. The core of SCR technology lies in the selection of excellent catalysts. The complex composition of flue gas can easily deactivate and poison the catalysts. Especially for water and sulfur, SCR catalysts are more sensitive, which affects the life of the catalysts, and makes the cost of treatment and operation significantly higher [144–146]. SCR technology is a method of selectively reducing NO_x to nitrogen and water by using ammonia or hydrocarbon or carbon monoxide as reductant under certain temperature and catalyst [147,148]. SCR is the most mature and widely used denitrification technology with high denitrification efficiency. It is the most efficient means to control NO_x pollution. Generally, the denitrification efficiency can reach 80–90% based on the rational selection of reactor and catalyst [149].

4.2.1. NH₃-SCR

NH₃-SCR is one of most efficient processes for denitrification. Up to date, NH₃-SCR systems have been widely applied in stationary industrial installations (SIIs), such as power plants and industrial boilers. Commercial vanadium-based catalysts usually work in the temperature range of 300 to 400 °C, and often suffer from high dust and SO₂ contents in flue gases, while a manganese-based monolithic honeycomb catalyst (MHC) showed high activity in NH₃-SCR at room temperature (as low as 20 °C). We believe that this room temperature NH₃-SCR technology is effective for high concentration NO_x removal with great potential for applications in SIIs.

Current SCR denitration (De-NO_x) technologies come in three categories, high-temperature De-NO_x at high dust content, high-temperature De-NO_x at high SO₂ content, and low-temperature De-NO_x at high H₂O content, as shown in Figure 9. These applications are particularly challenging

because of the varying operation conditions of SIIs with regard to flue gas temperature. The general niches and limitations of monolithic honeycomb catalysts (MHCs) for SCR processes and practical NO_x removal can be highlighted as follows.

- (i) High-temperature De- NO_x unit at high dust content. In this unit, the temperature of the flue gas entering the NH_3 -SCR reactor is as high as 300–400 °C. This high temperature significantly favors the De- NO_x performance of most of the catalysts (e.g., vanadium-type-based catalysts) [150,151]. At present, this technology is the most widely used in SIIs. However, further progress in promising applications is still somewhat bottlenecked by (a) the high dust content in the flue gas, which easily leads to erosion and plugging holes in MHCs and (b) the high SO_2 content of the flue gas, leading to catalyst poisoning and deactivation. These limitations are yet to be overcome [152].
- (ii) High-temperature De- NO_x unit at high SO_2 content. In this unit, the temperature of the flue gas entering the NH_3 -SCR reactor ranges from 180 to 280 °C. A dust-removing apparatus is used to mitigate the erosion and plugging issues for longer service life of MHCs for NH_3 -SCR. Nevertheless, the high SO_2 content continues to raise greater worries for activity declining and shorter service life [153,154]. Most of manganese- and copper-based catalysts with high SO_2 resistance could be used in this process [155,156].
- (iii) Low-temperature De- NO_x unit at high H_2O content. In this unit, the temperature of the flue gas entering the NH_3 -SCR reactor is below 160 °C. Although dust and SO_2 are previously removed, the H_2O content in the flue gas still remains as high as 10 vol.%. Almost all current catalysts show low activity and poor water-resistance at this temperature [157,158]. Therefore, this technique is not practical for SIIs.

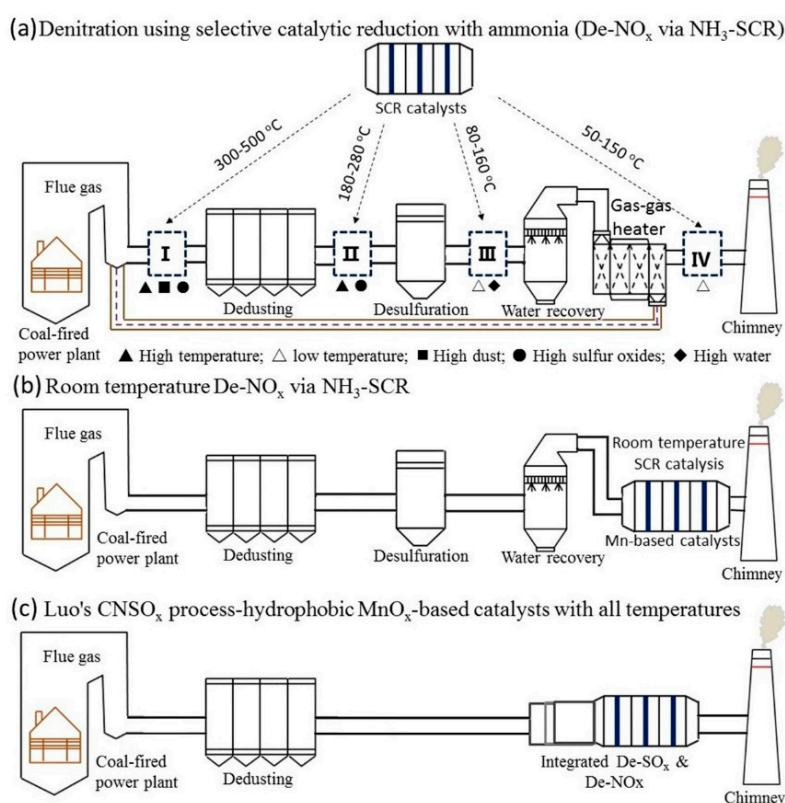


Figure 9. (a) Design route for De- NO_x via NH_3 -SCR. (I) high-temperature at high dust content, (II) high-temperature at high SO_2 content, (III) low-temperature at high H_2O content, and (IV) low temperature with water removal. (b) Room temperature De- NO_x via NH_3 -SCR. (c) Luo's process for treating CO , NO_x , and SO_x [159]. Reproduced from Ref. [159], Copyright 2018, Elsevier.

Additionally, in the process of low-temperature De-NO_x unit after H₂O removal, the water vapor in the flue gas is condensed and recovered. Furthermore, the flue gas obtained after the dust removal, desulfurization, and water recovery steps can be heated to a temperature ranging from 50 to 150 °C, depending on the flue gas flow. Most Mn-based catalysts exhibit great NH₃-SCR performance at low temperature [160]. This technique has potential in application for SIIs; however, the NO removal at low temperature still exists as a big challenge.

Zhang et al. [161] found inspiring room temperature De-NO_x performance in NH₃-SCR with Mn-based MHCs. The MnO_x-Fe₂O₃/vermiculite (VMT) catalyst showed high N₂ selectivity of 97.1% at 20 °C. The corresponding MnO_x-Fe₂O₃/VMT MHC exhibited a NO conversion of 62.2% at NO content of 500 ppm. Additionally, MnO_x-Fe₂O₃/VMT MHC showed excellent SO₂ resistance even at SO₂ content of 300 ppm, at which sulfate might be easily formed to foil the catalyst surface. As shown in Figure 8b, this room temperature NH₃-SCR technology is effective for high concentration NO_x removal, showing great potential for applications in SIIs.

For low temperature NH₃-SCR denitrification catalyst, it is very crucial to study denitrification mechanism for further improving its activity [162,163]. Ryu et al. [164] studied the location of active sites in NH₃-SCR reaction, mainly at Lewis acid sites on the catalyst surface. Campisi et al. [165] functionalized HAP by ion exchange. The high dispersion of Fe³⁺ species ensured the acid and redox centers. Yang et al. [166] studied the mechanism of NH₃-SCR reaction of NO on CuMn₂O₄ catalyst. Density functional theory calculation showed that the dehydrogenation of NH₃ was the decisive step of N₂ formation. Wu et al. [167] used hydrotalcite-like precursor to induce the modification of NiO by titanium dioxide (Figure 10a), which produced a good interface effect in the calcination process (Figure 10b). The active components were dispersed at atomic level, and the conversion rate was over 90% in the temperature range of 240 to 360 °C (Figure 10c,d).

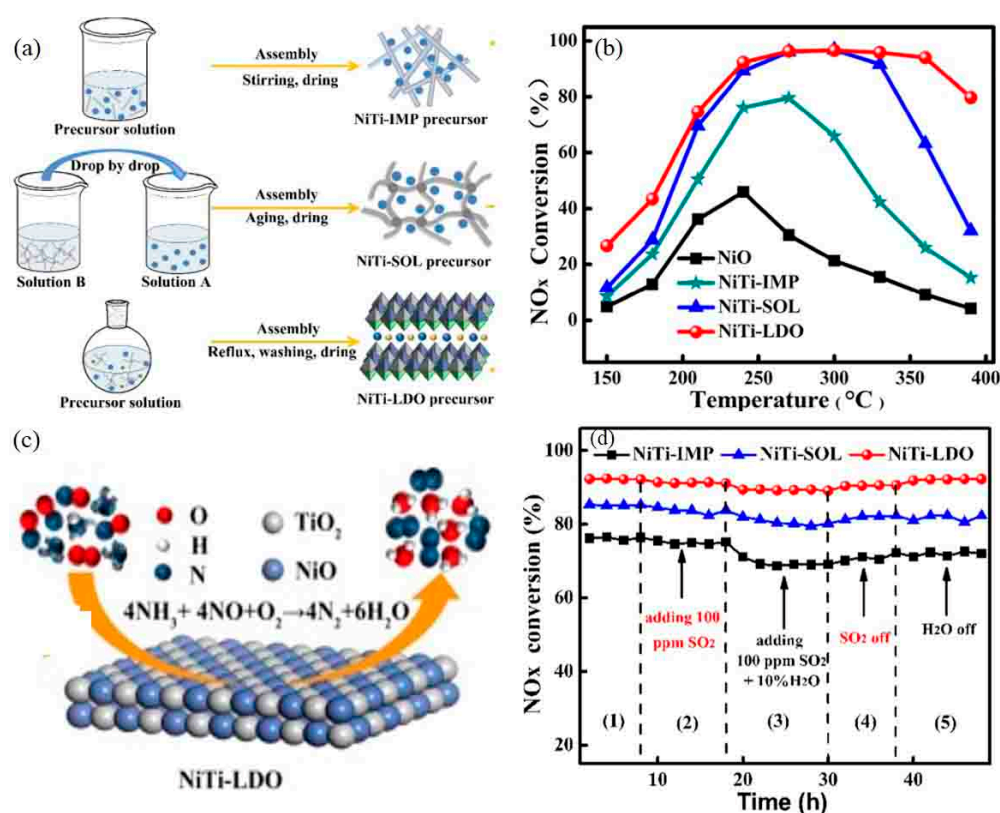


Figure 10. (a) Different preparation processes of Ni-Ti hydrotalcite-like precursors, (b) NO conversion of catalysts obtained by different preparation processes, (c) mechanism of NO removal induced by TiO₂ on the surface of NiO modified catalysts, and (d) sulfur resistance of Ni-Ti hydrotalcite-like precursors at 240 °C [167]. Reproduced from Ref. [167], Copyright 2019, Elsevier.

MnO_x-based catalysts are currently the focus of low-temperature NH₃-SCR flue gas denitrification technology research [168–170]. As an active component, MnO_x can provide free electrons, which play an important role in the SCR process [171]. Wang et al. [172] prepared MnO_x catalyst with Na₂CO₃ as precipitator has a high specific surface area and amorphous framework structure. Zhang et al. [173] synthesized Fe modified MnO_x/TiO₂ catalyst by sol–gel method; when the flue gas was simulated at 250 °C, the NO conversion reached 76.8%. Wang et al. [174] developed a MnO_x-CeO₂-Al₂O₃ catalyst with enhanced activity and good water resistance by using instantaneous nano-precipitation technology. Xiang et al. [175] discussed the adsorption mechanism of NH₃ and NO on MnO_x-based catalysts supported on γ-Al₂O₃. Wang et al. [176] studied the performance of a series of W-modified MnO_x/TiO₂ catalysts for NH₃-SCR. In situ infrared spectroscopy showed that more Brønsted and Lewis acid sites were formed on the catalyst surface after tungsten doping. Zhang et al. [177] studied the effect of Ce-Mo modified TiO₂ adsorbent on NO adsorption. Zhao et al. [178] prepared two-dimensional layered MnAl double oxides by instantaneous nanoprecipitation. Wang et al. [179] prepared MnO_x-CeO₂-Al₂O₃ catalysts with different MnO_x content by self-propagating high-temperature synthesis firstly, and the effects of different synthesis methods on NO conversion were compared in Table 4.

Table 4. Effects of different synthetic methods on de-NO_x activity of NH₃-SCR.

Catalyst	Synthetic Method	GHSV (hr ⁻¹)	Temperature (°C)	Conversion (%)	Ref.
Ce-Mo/TiO ₂	Coprecipitation	19,000	200–400	90	[177]
MnAl/LDO	FNP	60,000	150–250	100	[178]
MnO _x -CeO ₂ -Al ₂ O ₃	self-propagating synthesis	15,384	50–400	100	[179]
Mn–Ce–Ti	Hydrothermal	64,000	150–400	98	[180]
MnO _x -CeO ₂ -TiO ₂	Sol-ge	10,000	100–300	90	[181]
Co/Ni-CeO ₂	Coprecipitation	48,000	75–200	93	[182]
Fe-Mn–Ce/γ-Al ₂ O ₃	Sol-ge	10,000	100–450	95	[183]
MnO _x /CeO ₂ -ZrO ₂ -Al ₂ O ₃	Impregnation	10,000	50–300	90	[184]

The powder catalyst in the laboratory stage is quite mature, meaning it can efficiently remove nitrogen oxides from simulated flue gas. However, how to apply these excellent catalysts to practice is a question worthy of consideration. Obviously, powder catalysts must be prepared as monolith catalysts to meet the needs of stationary industrial installations. Monolith catalysts have many dominant positions, such as strong mechanical stability, thermal conductivity, mass transfer capacity, small pressure drop and recycling, which are conducive to the catalytic process and practical application.

Yu Feng research group of Shihezi University has studied the monolith catalyst deeply. Tian et al. [185] prepared nanoporous microspheres Mn–Ce–Fe–Ti mixed oxide catalysts for NH₃-SCR by spray drying (Figure 11a). The samples were processed by focused ion beam (FIB) and observed by scanning electron microscopy (Figure 11b,c). After application in flue gas treatment, it was found that the monolith catalyst still maintained good catalytic activity. Wang et al. [159] first designed and prepared spherical MnO_x-CeO₂-Al₂O₃ powder catalysts by spray drying, then applied it to monolith honeycomb catalysts(MHC). Compared with the same metal oxides catalysts prepared by coprecipitation (CP-MHC), the spray-drying (SD-MHC) method exhibited excellent SCR denitrification performance at 50–150 °C (Figure 11d,e).

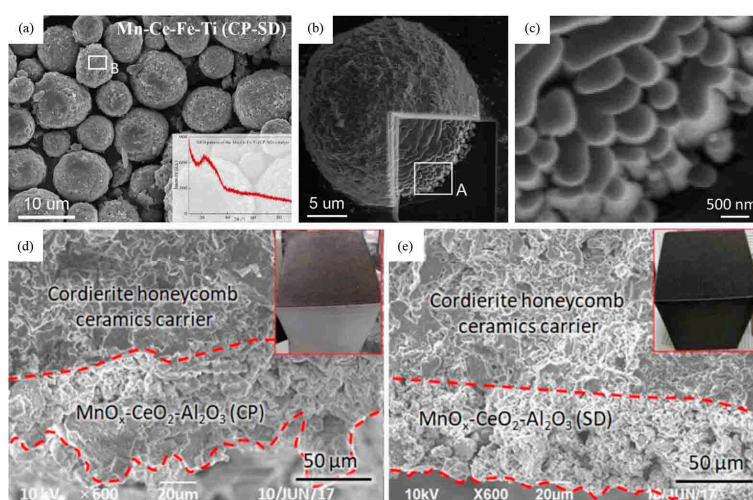


Figure 11. (a) The SEM image of nanoporous microspheres Mn-Ce-Fe-Ti mixed oxide catalysts, (b) focused ion beam (FIB) images and (c) SEM image of nanoporous microspheres Mn-Ce-Fe-Ti [185], (d) SEM images of MnO_x-CeO₂-Al₂O₃ (CP-MHC), and (e) MnO_x-CeO₂-Al₂O₃ (SD-MHC) [159]. Reproduced from Ref. [159], Copyright 2018, Elsevier.

4.2.2. CO-SCR

CO-SCR denitrification technology can effectively remove NO and CO from flue gas, thus performing two steps simultaneously [186]. In addition, CO-SCR as reducing agent can simultaneously remove NO and CO from tail gas and reduce the cost of purchase, transportation and storage of additional reducing agent. It is an attractive and promising denitrification technology. Therefore, it is urgent to study CO-SCR technology [187–189]. Besides, precious metals are expensive, have limited reserves and have poor high temperature performance. They sinter at about 800 °C. At the same time, they have poor sulfur and phosphorus resistance, so it is particularly important to develop non-precious metal catalysts. Current research focuses on rare earth elements and cheap transition metals, rare earth elements, especially Ce, are widely studied in cheap transition metals, such as Cu, Fe, Mn, etc. [190–192].

In order to further explore the performance of CO-SCR denitrification, Shen et al. [187] found that the operating temperature window moved towards low temperature after Fe co-doping with Mn-Ce/TiO₂. Yang et al. [193] studied the application of gas sensor in denitrification. Chen et al. [194] studied the CO+NO reaction on Pd/Al₂O₃ and Pd/CeZrO₂ catalysts. Cheng et al. [195] prepared Pd/LaFeO₃ nanoparticle catalysts supported on LaFeO₃ by two-step precipitation-deposition method. The visible light-induced valence exchange of Fe²⁺ and Fe³⁺ can promote the formation of oxygen vacancies. Lopes et al. [196] synthesized Cu-Ni catalyst by coprecipitation method. Bánsági et al. [197] found that isocyanate was the intermediate in the process of CO-SCR reaction. Wang et al. [198] studied the reaction of CO-SCR and the decomposition of supported metals by TG-FTIR. Liu et al. [190] prepared Cu_{0.1}La_{0.1}Ce_{0.8}O catalyst, which had good water resistance and catalytic stability in CO-SCR process. Yamashita et al. [199] studied the CO-SCR reaction of nickel species supported on silica. Yao et al. [200] discussed the mechanism of CeO₂ modified MnO_x catalyst at low temperature (Figure 12a). Phase interfaces or synergies were formed on the surface (Figure 12b). Jin et al. [201] further studied the sulfur resistance and water resistance of Mn-Mo-WO_x/TiO₂-SiO₂ catalysts. It was found that the catalytic activity of Mn-Mo-WO_x/TiO₂-SiO₂ catalysts decreased significantly when H₂O and SO₂ existed simultaneously (Figure 12c,d), and the effects of different synthesis methods on NO conversion were compared in Table 5.

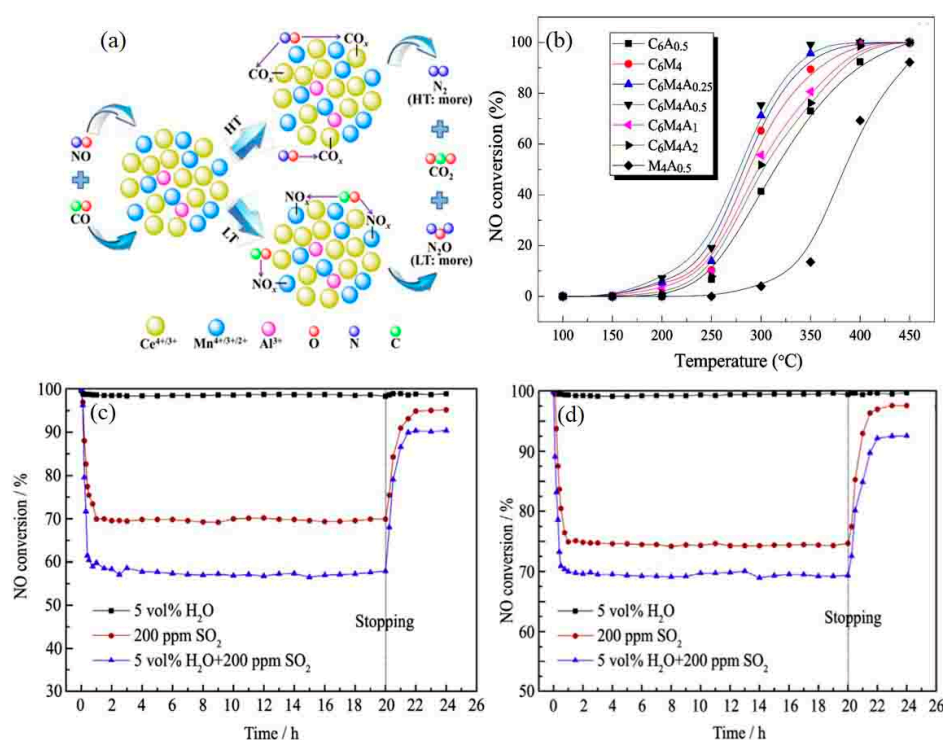


Figure 12. (a) The mechanism of selective catalytic CO removal from CeO₂-MnO_x-Al₂O₃ surface, (b) NO conversion of Ce-Mn/Al₂O₃ catalyst [200] (Reproduced from Ref. [200], Copyright 2016, Elsevier.), and (c,d) Mn-Mo-WO_x/TiO₂-SiO₂ catalyst CO-SCR for sulfur and water resistance [201]. (Reproduced from Ref. [201], Copyright 2018, Elsevier.)

Table 5. Effects of different synthetic methods on de-NO_x activity of CO-SCR.

Catalyst	Synthetic Method	Reaction Conditions	Temperature (°C)	NO Conversion (%)	Ref.
Cu _{0.1} La _{0.1} Ce _{0.8} O	Grind	500 ppm NO, 1000 ppm CO, GHSV 26,000 h ⁻¹ , Ar	250	99.2	[190]
Mn-Ce/TiO ₂	wetness impregnation	600 ppm NO, 1200 ppm CO, GHSV 40,000 h ⁻¹ , N ₂	200	94.9	[187]
Pd/CeZrO ₂	Impregnation	5 vol.% NO, 10 vol.% CO, GHSV 24,000 h ⁻¹ , He	300	100	[194]
Pd/LaFeO ₃	Two-step precipitation	5% NO, 10% CO, Water 10%, 24,000 mL h ⁻¹ , He	120	98	[195]
Cu-Ni/LDH	Precipitation	1.5 vol.% CO, 0.2 vol.% NO, O ₂ 0.65 vol.%, 12,000 h ⁻¹ , He	400	100	[196]
Fe _{0.8} Co _{0.2} /ASC	Precipitation	500 ppm NO, 1000 ppm CO, GHSV 40,000 h ⁻¹ , N ₂	200	96	[198]

4.2.3. HC-SCR

In recent years, selective catalytic reduction of hydrocarbons (HC-SCR) has become a hot research topic worldwide. It has potential advantages in large-scale flue gas emission control, diesel engine and lean combustion engine exhaust gas treatment. At present, many studies have focused on Ag/Al₂O₃ catalytic system. Compared with the transition metal catalysts represented by Cu, Ag/Al₂O₃ catalysts have higher NO conversion and N₂ selectivity, outstanding thermal stability, water sulfur resistance, which makes it to be one of the most promising catalysts for HC-SCR.

H₂ can significantly promote the HC-SCR by hydrocarbons. Xu et al. [202] studied the sulfur resistance of Ag/Al₂O₃ catalyst assisted by H₂. It was found that Ag/Al₂O₃ catalyst with higher Ag loading had better denitrification and sulfur resistance, especially 4% Ag/Al₂O₃ catalyst, which was

attributed to the rapid migration of sulfate on its surface to form more active sites. Thomas et al. [203] found that in the presence of H_2 , the stability of nitrate was greatly reduced, and H_2 greatly reduced the temperature of formation and decomposition of NO_x . Xu et al. [204] found that Ag/Al_2O_3 catalyst had excellent water resistance in the whole temperature range. After introducing water vapor, especially at low temperature, the conversion of NO_x was enhanced. Chaieb et al. [205] studied the reaction mechanism of H_2 assisting C_3H_6 to remove NO_x on Ag-loaded Al_2O_3 surface (Figure 13a). When the Ag-loading density reached $0.7Ag/nm^2Al_2O_3$, the contact process between NO and C_3H_6 was the decisive step of C_3H_6 -SCR process (Figure 13b). Xi et al. [206] prepared Fe-Ag/ Al_2O_3 catalyst loaded on cordierite by sol-gel method and impregnation method. After Fe modification, the catalyst surface became loose and porous, forming Fe_3O_4 -based needle-like and flaky crystals. It was found that Fe could effectively improve the performance of the catalyst against SO_2 and H_2O (Figure 13c,d), and increased the catalyst Lewis acid sites.

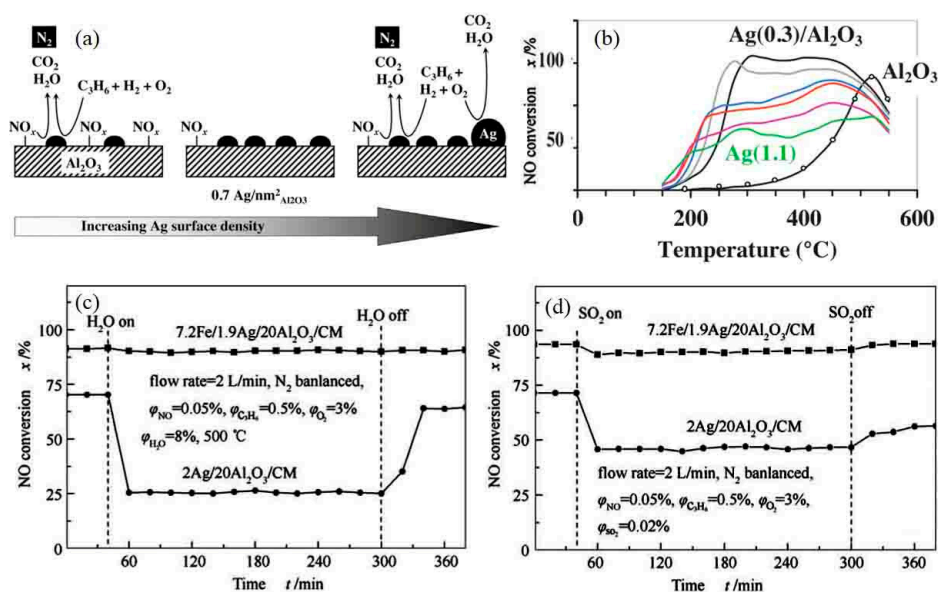


Figure 13. (a) The mechanism of C_3H_6 selective catalytic NO removal on Ag/Al_2O_3 surface, (b) the effect of Ag loading on NO conversion [205], and (c,d) the effect of Fe doping on the sulfur resistance and water resistance of Ag/Al_2O_3 catalyst [206]. Reproduced from Ref. [206], Copyright 2017, Elsevier.

4.2.4. H_2 -SCR

H_2 is the most clean and resource-rich reductant for selective catalytic removal of NO_x . Compared with traditional NH_3 and urea as reductant, hydrogen as reductant has the advantages of low reaction temperature, clean and no secondary pollution, and low temperature activity of H_2 -SCR catalyst.

Platinum and palladium, as unique active components, have excellent denitrification performance in the H_2 -SCR system. Wang et al. [207] prepared Pt/HZSM-5 catalyst by impregnation method. FTIR analysis showed that Pt on the outer surface of molecular sieve acted as an activation agent for H_2 in H_2 -SCR. Xue et al. [208] directly deposited Pt with different content on MIL-96 (Al) surface by hydrothermal method. Pt was slightly loaded on MIL-96 (Al) surface and H_2 -SCR catalytic activity was excellent at $80\text{ }^\circ\text{C}$. Zhang et al. [209] modified H_2 -SCR on Pt/HZSM-5 catalyst by tungsten doping. The results showed that tungsten was beneficial to the metal state of platinum in the catalyst and inhibited the formation of nitrate. At the same time, tungsten accelerated the dissociation of nitric oxide on the platinum surface. Väliheikki et al. [210] found that tungsten doping could improve the catalytic activity through the acidity of $Ce_zZr_{1-z}O_2$ surface on H_2 -SCR catalyst. Yang et al. [211] studied the catalytic performance of platinum supported on H-ferrous acid. In situ infrared spectroscopy showed that NO_2 and nitrate were not important intermediates of H_2 -SCR on the catalyst, while $NO^{\delta+}$ on Pt was an effective material for NO removal. Huai et al. [212] studied the decomposition process of

NO on Pd (111) surface and the formation pathways of N_2 , NH_3 , N_2O , and H_2O (Figure 14a,b). The specific temperatures of them could be obtained by relative selectivity analysis at different temperatures (Figure 14c,d).

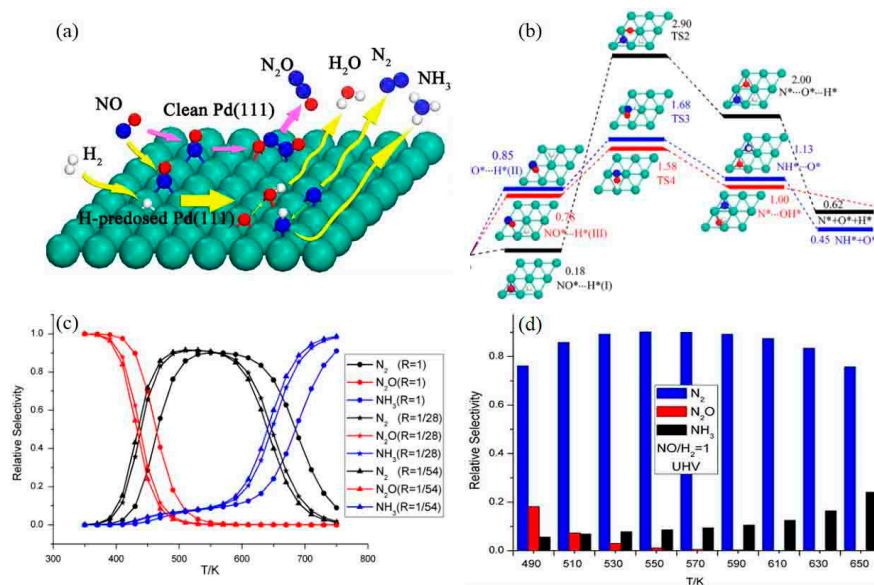


Figure 14. (a) Reaction pathways of NO + H₂ and products on Pd (111), (b) potential energy diagram and geometrical structure of H atom-assisted direct dissociation of NO on Pd (111), and (c,d) relative selectivity of N₂, NH₃, N₂O, and H₂O at different temperatures [212]. Reproduced from Ref. [212], Copyright 2015, Elsevier.

Removal of NO_x by reduction is an extraordinary efficient method for removing NO_x. However, SCR is limited by a series of problems, such as high cost, high temperature at 300 °C, NH₃ escaping from secondary pollution environment [213], poor sulfur and water resistance of catalysts and susceptibility to poisoning and inactivation [214,215], which affect the life of the catalysts, makes the treatment and operation cost significantly higher [216,217]. Therefore, how to promote the resource-saving and environmentally friendly denitrification process is a difficult problem to be solved urgently in the world [218]. Studying the reaction mechanism of NO on catalyst surface is of great significance for solving the problem of catalyst poisoning and deactivation; improving catalytic denitrification activity; promoting dust, H₂O, and SO₂ resistance; enlarging operation temperature window; and promoting the low temperature direction of reaction [219–221].

5. Removal of NO_x by Plasma

Plasma was discovered by German physicist and chemist Krux in 1879 and was first introduced into physics by American scientists Langmuir and Tonks. The plasma is the fourth form of matter, which contains a large number of electrons, ions, molecules, neutral atoms, excited state atoms, photons, and free radicals, among which positive and negative ions have the same charge [222]. Strictly speaking, plasma is a gas mass with high potential kinetic energy. The total charged quantity of plasma is still neutral. The outer electrons are shot out by the high kinetic energy of electric field or magnetic field. As a result, electrons are no longer bound to the nucleus, but become free electrons with high potential and high kinetic energy [223,224]. The plasma is a good conductive fluid, and there is no net Coulomb force or net magnetic force between charged particles. The charged particles are positive and negative in microscopy and electrically neutral in macro, and have certain thermal effects. According to the different thermodynamic equilibrium states, plasma can be divided into thermodynamic equilibrium plasma and non-thermodynamic equilibrium plasma [225,226]. Thermodynamically balanced plasma, also known as high temperature plasma, has the same temperature of molecule, electron and ion [227].

5.2. Plasma-Modified Catalyst

NO_x removal by plasma-modified catalysts is a new green and environmental technology. The modification of catalysts by plasma is mainly focused on the surface modification of catalysts. The dispersion of active species can be improved by plasma modification, and the stability and low temperature activity of catalysts can be improved [242]. Hong et al. [243] studied the denitrification performance of pulsed corona discharge plasma. The results showed that there was an obvious interaction between the process of desulfurization and denitrification. Zhang et al. [244] treated $\text{NiO-TiO}_2\text{-Al}_2\text{O}_3$ catalyst with plasma. It was found that the specific surface area of the catalyst was increased, the nickel particles dispersed more evenly and the ability of the catalyst to adsorb NO_x was enhanced. Huang et al. [245] prepared $\text{V}_2\text{O}_5/\text{ACF}$ catalyst. After oxygen plasma modification, the surface oxygen-containing functional groups increased, the pore size distribution widened and the catalytic activity increased. Liu et al. [246] prepared a Mn-O-Ce catalyst by nonthermal plasma, it decomposes nitrate and organic matter slowly and forms defective Mn-O-Ce phase in the catalyst during plasma treatment. More details are shown in Table 6.

Table 6. The performance contrast of plasma-modified catalysts.

Catalyst	Conversion (%)	Temperature (°C)	Ref.
$\text{NiO-TiO}_2\text{-Al}_2\text{O}_3$	Without plasma < 12 Plasma-modified > 70	180–240	[244]
$\text{V}_2\text{O}_5/\text{ACF}$	Without plasma < 35 Plasma-modified > 55	50–150	[245]

The plasma contains high energy, which can provide enough activation energy for many difficult reactions. An et al. [247] studied the oxidation characteristics of NO in oxygen atmosphere by surface dielectric barrier discharge plasma treatment of mixed flue gas with active material injection method. Cui et al. [248] prepared a MnCe/Ti catalyst in a dielectric barrier discharge reactor by combining nonthermal plasma discharge with catalyst. The highest NO conversion rate was 86.9%. Zhao et al. [249] developed a new process of denitrification by water-cooled dielectric barrier discharge. Peng et al. [250] used nonthermal plasma and bamboo charcoal combined with adsorption technology to catalyze the removal of NO. SEM showed that the surface of the catalyst after plasma treatment would produce defects to promote the growth of pore structure and increase the active sites. Park et al. [251] removed both NO and SO_2 from flue gas through a wet NaClO_2 scrubber combined with a plasma electrostatic precipitator. Wang et al. [252] prepared Mn–Ce/ZSM5 multi-walled carbon nanotubes catalyst by impregnation (Figure 16a). It was found that more oxygen holes could be generated after plasma treatment, which could significantly improve NO conversion (Figure 14b). Among them, $\text{Mn}_1\text{Ce}_1/\text{ZSM5}$ has the highest catalytic activity and its reaction accorded with Eley–Rideal mechanism (Figure 16c). The sulfur and water resistance of $\text{Mn}_1\text{Ce}_1/\text{ZSM5}$ were also slightly improved (Figure 16d).

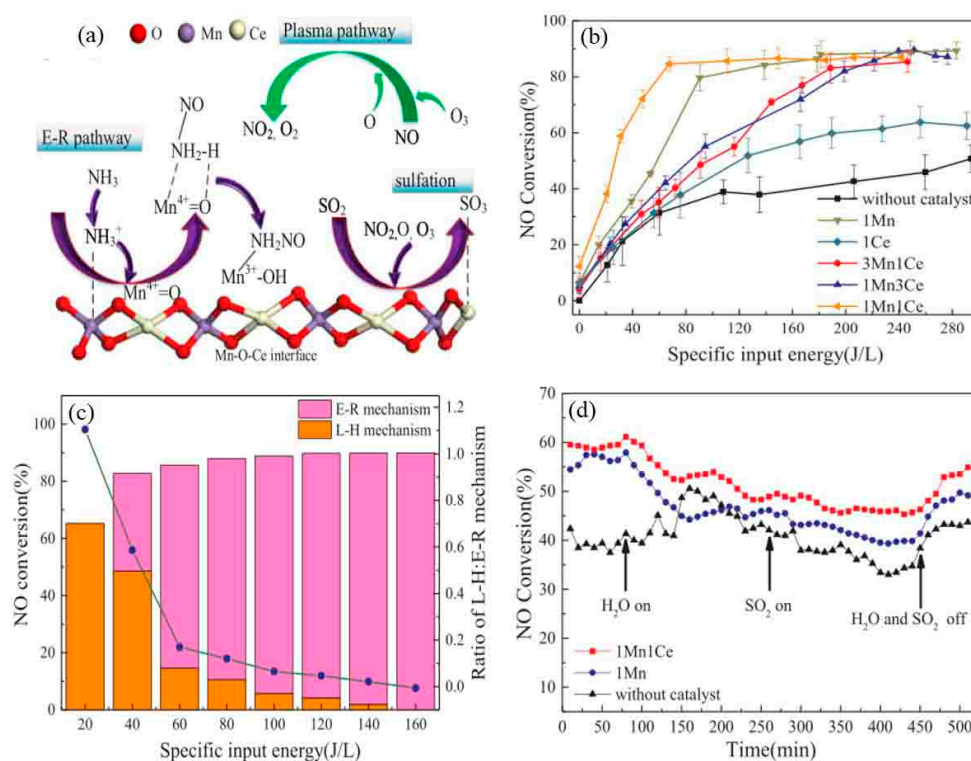


Figure 16. (a) Mechanism of NO_x removal by plasma-modified catalyst Mn-Ce/ZSM5, (b) effect of different Mn-Ce ratios and plasma treatment on NO conversion, (c) denitrification process of catalyst Mn₁Ce₁/ZSM5 conforms to Eley-Rideal mechanism, and (d) study on sulfur and water resistance of plasma-modified catalyst [252]. Reproduced from Ref. [252], Copyright 2018, Elsevier.

5.3. Plasma Concerted Catalysis

Plasma concerted catalysis is the combination of plasma and catalyst, which makes them act synergistically on the reaction system and optimize the reaction process. According to the combination of catalysts and plasma, plasma-assisted catalysis can be divided into plasma-enhanced catalysis and plasma-driven catalysis. (1) Plasma-enhanced catalysis: catalysts work at the back of the plasma and the plasma and catalyst work in the optimum temperature range respectively. Under this combination mode, the role of plasma is to change the gas composition reaching the catalyst bed. Reactive gases are treated by plasma to produce more highly active intermediates, which react on catalysts to produce final products [253]. (2) Plasma-driven catalysis: plasma and catalyst are placed in the same reactor, and a large number of short-lived active species produced by plasma change the shape of gaseous reactants on the catalyst. The discharge of plasma on the catalyst surface may also change the properties of the catalyst, such as the generation of electron holes and electrons, and the surface of the catalyst. The change of work function, the activation of lattice oxygen of catalyst, the formation of new active sites on catalyst surface, etc. [254]. Tang et al. [255] studied the effect of nonthermal plasma co-catalytic treatment on the low-temperature oxidation of NO by Mn-CoO_x catalyst (Figure 17a,b). It was found that the activity of the catalyst treated by nonthermal plasma increased significantly (Figure 17c), and the specific surface area and pore volume of the catalyst increased significantly after nonthermal plasma treatment, as well as the advantages of changing the relative surface concentration and oxidation state of the species on the catalyst surface. Two main weightlessness peaks were studied (Figure 17d).

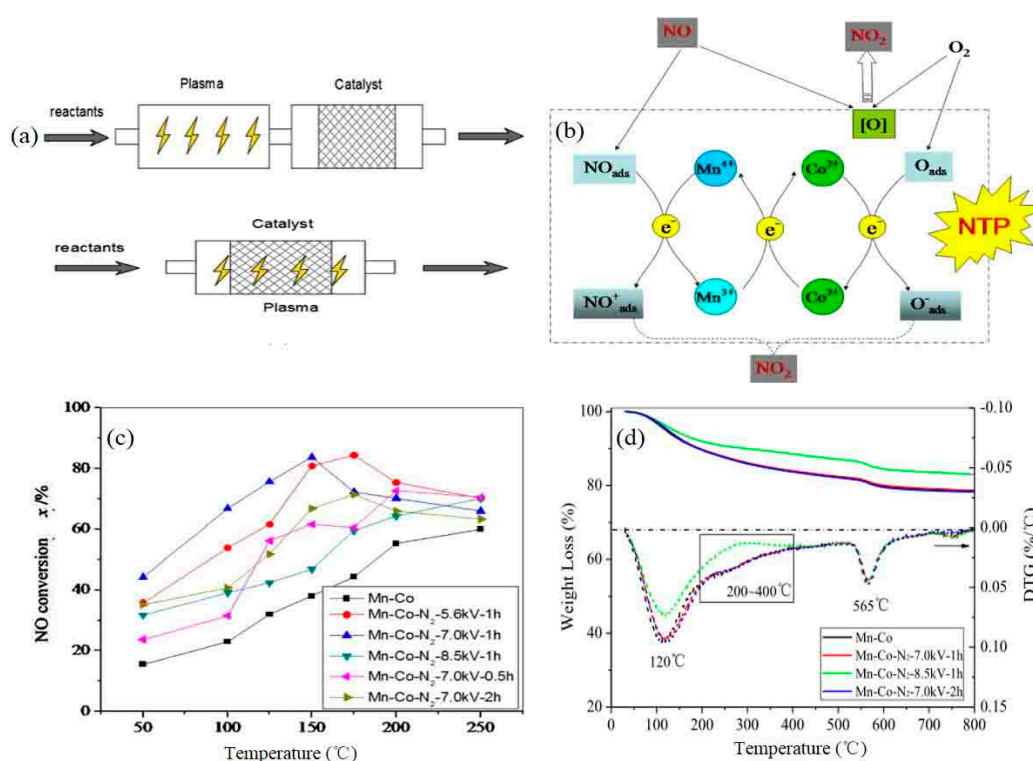


Figure 17. (a) Schematic diagram of plasma-enhanced catalysis and plasma-driven catalysis, (b) mechanism of low-temperature denitrification of nonthermal plasma-enhanced Mn-CoO_x catalyst, (c) effect of plasma voltage and treatment time on NO conversion, and (d) study on thermal stability of thermogravimetric curves [255]. Reproduced from Ref. [255], Copyright 2015, Elsevier.

To further demonstrate the concerted effect of plasma, the following data are listed to enhance persuasion. Niu et al. [256] found that the denitrification rate was greatly increased when the plasma acted with Co-ZSM-5 zeolite catalyst. Bröer et al. [257] found that the activity of SCR at low temperature increased significantly under the action of plasma with V₂O₅-WO₃/TiO₂ catalyst. Fan [258] studied the concerted effect of plasma and H₂ mordenite in C₂H₂-SCR. Li et al. [259] explored the enhanced effect of Mn-Co-CeO_x catalyst with plasma treatment in NH₃-SCR. Cho et al. [260] discussed the concerted effect in plasma-enhanced catalysis. Using Ba & Cu (C₂H₂O₃)₂ as catalyst, NO was oxidized to NO₂ in plasma, while hydrocarbon was oxidized to active intermediate species CO, which eventually reduced NO_x to N₂. Pan et al. [261] found that the conversion of NO_x as well as the water and sulfur resistance of C₃H₈-SCR plasma increased significantly when dielectric barrier plasma acted simultaneously. Wang et al. [262,263] found that the denitrification rate was very low when the plasma acted alone. When the plasma cooperated with the Mn-Cu/ZSM5 zeolite catalyst, the conversion of NO was greatly increased. The above data are summarized in Table 7.

In recent years, the form of plasma has been innovated rapidly [264,265]. Dielectric barrier discharge, radio frequency discharge, and microwave discharge are all new nonthermal equilibrium plasma discharge forms [266,267]. The effect of plasma denitrification is remarkable, which can improve the NO conversion rapidly on short notice. However, compared with the traditional denitrification technology, the plasma process has made some progress, but there are still some problems: high energy consumption, short power supply life and performance to be improved; moreover, the expensive price of plasma equipment, high cost of system operation and maintenance, and complex equipment structure make the technology not widely used and restrict its development.

Table 7. Effect of plasma addition on denitrification activity of different catalysts.

Catalyst	Conversion (%)	Temperature (°C)	Ref.
Co-ZSM-5	Plasma only 12	150–450	[256]
	Catalyst only 85	300	
	Plasma assist catalyst 95	300	
V ₂ O ₅ -WO ₃ /TiO ₂	Plasma only 20	150–260	[257]
	Catalyst only 35	180–260	
	Plasma assist catalyst 80	160–260	
H-mordenite	Plasma only 3.8	200	[258]
	Catalyst only 54	200	
	Plasma assist catalyst 91.4	200	
Mn-Co-CeO ₂	Plasma only 73	150	[259]
	Catalyst only 70	150	
	Plasma assist catalyst 93	100	
Ba & Cu (C ₂ H ₂ O ₃) ₂	Plasma only 85	25–400	[260]
	Catalyst only 82	25–400	
	Plasma assist catalyst 95	200	
Mn-CoO _x	Plasma only 3.8	200	[255]
	Catalyst only 54	200	
	Plasma assist catalyst 91.4	200	
Mn-Cu/ZSM5	Plasma only 50	25–450	[262]
	Catalyst only 60	25–450	
	Plasma assist catalyst 90	25	

6. Conclusions and Prospect

Along with the huge global emission of NO_x, which continues to deteriorate planet earth environment and human health in the Anthropocene, it becomes progressively significant to collect and summarize the efficient approaches of governance and treatment of NO_x. Optimizing the above four distinct denitrification methods and controlling the emission of NO_x are the main challenges for future atmospheric environmental treatment. Finally, in order to solve the problem of air pollution that plagues all countries in the world, the feasibility of four main technologies in the field of flue gas denitrification and industrial application of flue gas tail purify is evaluated.

Adsorption treatment of NO_x has the features of environmental friendliness, energy-saving, and high efficiency. The process is simple to operate, controllable, for low concentration poisonous gases, efficient capture can be achieved. However, due to their limited adsorption capacity, frequent regeneration of adsorbents, and huge size and the large-scale investment required, the application of adsorbents is limited. Oxidation process is a relatively mature method in the field of wet denitrification technology because of its simple route, easy operation and outstanding denitrification effect. Some of them have been industrialized. However, the oxidation tower has the problems of expensive raw materials and equipment corrosion, which limits its development due to its cost and safety. Reduction is the most efficient and mature denitrification technology with the most extensive application as well as the most exceptional means to control NO_x pollution. But at the same time, it has some shortcomings, high investment, high cost of catalyst regeneration, NH₃ escaping from secondary pollution, and poor sulfur and water resistance of catalyst and so on. The removal of NO_x by plasma technology is remarkable, which can rapidly improve the denitrification performance in a short time, and promote the stability and low temperature activity of the catalyst. However, the required equipment covers a large area, consumes high energy, and costs high investment, operation and maintenance, which is limited in practical application.

Future, the general requirement of denitrification technology is low cost, high efficiency and green. The overall development trend of technology is to realize the coordinated removal of multiple

pollutants by coupling multiple technologies. Different regions and industries are suitable for different denitrification means. In order to decrease the emission level of NO_x, cut down the expense of treatment and recovery, and improve the economic performance, different regions and industries should choose appropriate denitrification technology according from the resource situation to product usage. Therefore, it is of great practical significance to develop denitrification methods with high efficiency, low energy consumption, low secondary pollution, and low investment.

Author Contributions: F.Y. and B.D. provided framework. Z.L. summarizes the content of the article. C.M., J.D. and J.L. collected information.

Funding: The work was supported by Major Scientific and Technological Project of Bingtuan (No. 2018AA002), the National Natural Science Foundation of China (21663022), and Science and Technology Innovation Talents Program of Bingtuan (No. 2019CB025)

Conflicts of Interest: The authors declare no conflicts of interest.

References

1. Seitzinger, S.P.; Phillips, L. Nitrogen stewardship in the Anthropocene. *Science* **2017**, *357*, 350–351. [[CrossRef](#)] [[PubMed](#)]
2. Tvw, J.; Pnr, V. A molecular dance to cleaner air. *Science* **2017**, *357*, 866–867.
3. Boyle, E. Nitrogen pollution knows no bounds. *Science* **2017**, *356*, 700. [[CrossRef](#)] [[PubMed](#)]
4. Anenberg, S.C.; Miller, J.; Minjares, R.; Du, L.; Henze, D.K.; Lacey, F.; Malley, C.S.; Emberson, L.; Franco, V.; Klimont, Z. Impacts and mitigation of excess diesel-related NO_x emissions in 11 major vehicle markets. *Nature* **2017**, *545*, 467. [[CrossRef](#)] [[PubMed](#)]
5. Lelieveld, J.; Evans, J.S.; Fnais, M.; Giannadaki, D.; Pozzer, A. The contribution of outdoor air pollution sources to premature mortality on a global scale. *Nature* **2015**, *525*, 367–371. [[CrossRef](#)]
6. McDonald, B.C.; de Gouw, J.A.; Gilman, J.B.; Jathar, S.H.; Akherati, A.; Cappa, C.D.; Jimenez, J.L.; Lee-Taylor, J.; Hayes, P.L.; McKeen, S.A.; et al. Volatile chemical products emerging as largest petrochemical source of urban organic emissions. *Science* **2018**, *359*, 760. [[CrossRef](#)] [[PubMed](#)]
7. Zhao, C.N.; Xu, Z.; Wu, G.C.; Mao, Y.M.; Liu, L.N.; Qian, W.; Dan, Y.L.; Tao, S.S.; Zhang, Q.; Sam, N.B.; et al. Emerging role of air pollution in autoimmune diseases. *Autoimmun. Rev.* **2019**, *18*, 507–614. [[CrossRef](#)]
8. Schraufnagel, D.E.; Balmes, J.R.; Cowl, C.T.; De Matteis, S.; Jung, S.-H.; Mortimer, K.; Perez-Padilla, R.; Rice, M.B.; Riojas-Rodriguez, H.; Sood, A.; et al. Air Pollution and Noncommunicable Diseases: A Review by the Forum of International Respiratory Societies' Environmental Committee, Part 2: Air Pollution and Organ Systems. *Chest* **2019**, *155*, 417–426. [[CrossRef](#)]
9. Guo, T.; Wang, Y.; Zhang, H.; Zhang, Y.; Zhao, J.; Wang, Q.; Shen, H.; Wang, Y.; Xie, X.; Wang, L.; et al. The association between ambient PM_{2.5} exposure and the risk of preterm birth in China: A retrospective cohort study. *Sci. Total Environ.* **2018**, *633*, 1453–1459. [[CrossRef](#)]
10. Zeng, Q.; Darboux, F.; Man, C.; Zhu, Z.; An, S. Soil aggregate stability under different rain conditions for three vegetation types on the Loess Plateau (China). *CATENA* **2018**, *167*, 276–283. [[CrossRef](#)]
11. Du, E.; Dong, D.; Zeng, X.; Sun, Z.; Jiang, X.; de Vries, W. Direct effect of acid rain on leaf chlorophyll content of terrestrial plants in China. *Sci. Total Environ.* **2017**, *605*, 764–769. [[CrossRef](#)] [[PubMed](#)]
12. Bang, H.Q.; Nguyen, H.D.; Vu, K.; Hien, T.T. Photochemical Smog Modelling Using the Air Pollution Chemical Transport Model (TAPM-CTM) in Ho Chi Minh City, Vietnam. *Environ. Model. Assess.* **2019**, *24*, 295–310. [[CrossRef](#)]
13. Lewis, A.C. The changing face of urban air pollution. *Science* **2018**, *359*, 744. [[CrossRef](#)] [[PubMed](#)]
14. Wang, C.; Wang, W.; Sardans, J.; An, W.; Zeng, C.; Abid, A.A.; Peñuelas, J. Effect of simulated acid rain on CO₂, CH₄ and N₂O fluxes and rice productivity in a subtropical Chinese paddy field. *Environ. Pollut.* **2018**, *243*, 1196–1205. [[CrossRef](#)] [[PubMed](#)]
15. Song, Y.; Guo, S.; Zhang, M. Assessing customers' perceived value of the anti-haze cosmetics under haze pollution. *Sci. Total Environ.* **2019**, *685*, 753–762. [[CrossRef](#)] [[PubMed](#)]
16. Chong, X.; Wang, Y.; Liu, R.; Zhang, Y.; Zhang, Y.; Zheng, W. Pollution characteristics and source difference of gaseous elemental mercury between haze and non-haze days in winter. *Sci. Total Environ.* **2019**, *678*, 671–680. [[CrossRef](#)] [[PubMed](#)]

17. Li, C.; Wang, Y.; Jia, B.; Roskilly, A.P. Application of Miller cycle with turbocharger and ethanol to reduce NO_x and particulates emissions from diesel engine—A numerical approach with model validations. *Appl. Therm. Eng.* **2019**, *150*, 904–911. [[CrossRef](#)]
18. Gu, Y.; Epling, W.S. Passive NO_x adsorber: An overview of catalyst performance and reaction chemistry. *Appl. Catal. Gen.* **2019**, *570*, 1–14. [[CrossRef](#)]
19. Huang, R.; Zhang, S.; Ding, J.; Meng, Y.; Zhong, Q.; Kong, D.; Gu, C. Effect of adsorption properties of phosphorus-doped TiO₂ nanotubes on photocatalytic NO removal. *J. Colloid Interface Sci.* **2019**, *553*, 647–654. [[CrossRef](#)] [[PubMed](#)]
20. Hirai, T.; Okoshi, M.; Ishikawa, A.; Nakai, H. Temperature- and pressure-dependent adsorption configuration of NO molecules on Rh(111) surface: A theoretical study. *Surf. Sci.* **2019**, *686*, 58–62. [[CrossRef](#)]
21. Wang, T.; Ding, L.; Song, Y.; Cuiqing, L.I.; Wang, H.; Ren, X. Performance of simultaneous denitrification and desulfurization for Y₂O₃/AC catalysts. *Chin. J. Environ. Eng.* **2016**, *4*, 132–139.
22. Liu, Y.; Zhang, X.; Ding, J. Chemical effect of NO on CH₄ oxidation during combustion in O₂/NO environments. *Chem. Phys. Lett.* **2019**, *727*, 59–65. [[CrossRef](#)]
23. Zhang, T.; Li, H.; Yang, Z.; Cao, F.; Li, L.; Chen, H.; Liu, H.; Xiong, K.; Wu, J.; Hong, Z.; et al. Electrospun YMn₂O₅ nanofibers: A highly catalytic activity for NO oxidation. *Appl. Catal. Environ.* **2019**, *247*, 133–141. [[CrossRef](#)]
24. Jo, D.; Park, G.T.; Ryu, T.; Hong, S.B. Economical synthesis of high-silica LTA zeolites: A step forward in developing a new commercial NH₃-SCR catalyst. *Appl. Catal. Environ.* **2019**, *243*, 212–219. [[CrossRef](#)]
25. Chitpakdee, C.; Junkaew, A.; Maitarad, P.; Shi, L.; Promarak, V.; Kungwan, N.; Namuangruk, S. Understanding the role of Ru dopant on selective catalytic reduction of NO with NH₃ over Ru-doped CeO₂ catalyst. *Chem. Eng. J.* **2019**, *369*, 124–133. [[CrossRef](#)]
26. Yang, W.; Gao, Z.; Liu, X.; Ma, C.; Ding, X.; Yan, W. Directly catalytic reduction of NO without NH₃ by single atom iron catalyst: A DFT calculation. *Fuel* **2019**, *243*, 262–270. [[CrossRef](#)]
27. Wang, D.; Cheng, J.; Wang, B.; Lou, J.; Li, Y.; Li, X.; Li, Z.; Liu, X.; Meng, Q.; Gao, P.; et al. Plasma-catalytic high-efficiency oxidation of NO over Co-Mn/Ti catalysts using surface dielectric barrier discharge plasma. *Vacuum* **2019**, *167*, 249–254. [[CrossRef](#)]
28. Wang, J.; Yi, H.; Tang, X.; Zhao, S.; Gao, F. Exceptional adsorptive capacity and kinetic of γ-Al₂O₃ for selective adsorption of NO assisted by nonthermal plasma. *Chem. Eng. J.* **2019**, *378*, 122095. [[CrossRef](#)]
29. Xie, S.; Ren, W.; Qiao, C.; Tong, K.; Sun, J.; Zhang, M.; Liu, X.; Zhang, Z. An electrochemical adsorption method for the reuse of waste water-based drilling fluids. *Nat. Gas Ind. B* **2018**, *5*, 508–512. [[CrossRef](#)]
30. Ikeda, H.; Koike, Y.; Shiratori, K.; Ueda, K.; Shirahata, N.; Isegawa, K.; Toyoshima, R.; Masuda, S.; Mase, K.; Nito, T.; et al. Adsorption state of NO on Ir (111) surfaces under excess O₂ coexisting condition. *Surf. Sci.* **2019**, *685*, 1–6. [[CrossRef](#)]
31. Zhao, Y.; Wang, H.; Wang, T. Adsorption of NO from flue gas by molecularly imprinted adsorbents. *Chem. Eng. J.* **2016**, *306*, 832–839. [[CrossRef](#)]
32. Hastürk, E.; Ernst, S.J.; Janiak, C. Recent advances in adsorption heat transformation focusing on the development of adsorbent materials. *Curr. Opin. Chem. Eng.* **2019**, *24*, 26–36. [[CrossRef](#)]
33. Qu, W.; Yuan, T.; Yin, G.; Xu, S.; Zhang, Q.; Su, H. Effect of properties of activated carbon on malachite green adsorption. *Fuel* **2019**, *249*, 45–53. [[CrossRef](#)]
34. Szczeńniak, B.; Choma, J.; Jaroniec, M. Ultrahigh benzene adsorption capacity of graphene-MOF composite fabricated via MOF crystallization in 3D mesoporous graphene. *Microporous Mesoporous Mater.* **2019**, *279*, 387–394. [[CrossRef](#)]
35. Sherino, B.; Halim, S.N.A.; Manan, N.S.A.; Sarip, R.; Al'Abri, A.M.; Mohamad, S. Facile synthesis and characterization of novel dicarboxylate-Cu based MOFs materials. *Inorg. Chim. Acta* **2019**, *491*, 59–66. [[CrossRef](#)]
36. Qin, Y.H.; Huang, L.; Zhang, L.; He, H. One-step synthesis of confined ion Agx-Cu-BTC for selective catalytic reduction of NO with CO. *Inorg. Chem. Commun.* **2019**, *102*, 130–133. [[CrossRef](#)]
37. Khan, A.H.; Peikert, K.; Fröba, M.; Bertmer, M. NO adsorption in amino-modified Cu₃(btc)₂-type MOFs studied by solid-state NMR. *Microporous Mesoporous Mater.* **2015**, *216*, 111–117. [[CrossRef](#)]
38. Kaur, R.; Kaur, A.; Umar, A.; Anderson, W.A.; Kansal, S.K. Metal organic framework (MOF) porous octahedral nanocrystals of Cu-BTC: Synthesis, properties and enhanced adsorption properties. *Mater. Res. Bull.* **2019**, *109*, 124–133. [[CrossRef](#)]

39. Meng, G.; Song, X.; Ji, M.; Hao, J.; Shi, Y.; Ren, S.; Qiu, J.; Hao, C. Molecular simulation of adsorption of NO and CO₂ mixtures by a Cu-BTC metal organic framework. *Curr. Appl. Phys.* **2015**, *15*, 1070–1074. [[CrossRef](#)]
40. Qin, Y.H.; Huang, L.; Zhang, D.L.; Sun, L.G. Mixed-node A-Cu-BTC and porous carbon based oxides derived from A-Cu-BTC as low temperature NO–CO catalyst. *Inorg. Chem. Commun.* **2016**, *66*, 64–68. [[CrossRef](#)]
41. Li, Z.; Yu, Q.; Ying, C.; Fei, X.; Li, W.; Li, Y.; Chen, M. Adsorption properties of activated carbon from reed with a high adsorption capacity. *Ecol. Eng.* **2017**, *102*, 443–450.
42. Vanraes, P.; Ghodbane, H.; Davister, D.; Wardenier, N.; Nikiforov, A.; Verheust, Y.P.; Swih, V.H.; Hamdaoui, O.; Vandamme, J.; Van, D.J. Removal of several pesticides in a falling water film DBD reactor with activated carbon textile: Energy efficiency. *Water Res.* **2017**, *116*, 1–12. [[CrossRef](#)] [[PubMed](#)]
43. Beijer, K.; Björlenius, B.; Shaik, S.; Lindberg, R.H.; Brunström, B.; Brandt, I. Removal of pharmaceuticals and unspecified contaminants in sewage treatment effluents by activated carbon filtration and ozonation: Evaluation using biomarker responses and chemical analysis. *Chemosphere* **2017**, *176*, 342–351. [[CrossRef](#)] [[PubMed](#)]
44. Qu, G.; Kou, L.; Wang, T.; Liang, D.; Hu, S. Evaluation of activated carbon fiber supported nanoscale zero-valent iron for chromium (VI) removal from groundwater in a permeable reactive column. *J. Environ. Manag.* **2017**, *201*, 378. [[CrossRef](#)] [[PubMed](#)]
45. Shimabuku, K.K.; Paige, J.M.; Lunaaguero, M.; Summers, R.S. Simplified Modeling of Organic Contaminant Adsorption by Activated Carbon and Biochar in the Presence of Dissolved Organic Matter and Other Competing Adsorbates. *Environ. Sci. Technol.* **2017**, *51*, 10031–10040. [[CrossRef](#)] [[PubMed](#)]
46. Li, Y.; Duan, Y.; Hui, W.; Zhao, S.; Chen, M.; Meng, L.; Wei, H. Effects of Acidic Gases on Mercury Adsorption by Activated Carbon in Simulated Oxy-Fuel Combustion Flue Gas. *Energy Fuels* **2017**, *31*, 9745–9751. [[CrossRef](#)]
47. Sawant, S.Y.; Munusamy, K.; Somani, R.S.; John, M.; Newalkar, B.L.; Bajaj, H.C. Precursor suitability and pilot scale production of super activated carbon for greenhouse gas adsorption and fuel gas storage. *Chem. Eng. J.* **2017**, *315*, 415–425. [[CrossRef](#)]
48. Fałtynowicz, H.; Hodurek, P.; Kaczmarczyk, J.; Kułażyński, M.; Łukaszewicz, M. Hydrolysis of surfactin over activated carbon. *Bioorg. Chem.* **2019**, *13*, 145–149. [[CrossRef](#)]
49. Sajjadi, S.A.; Mohammadzadeh, A.; Tran, H.N.; Anastopoulos, I.; Dotto, G.L.; Lopičić, Z.R.; Sivamani, S.; Rahmani-Sani, A.; Ivanets, A.; Hosseini-Bandegharaei, A. Efficient mercury removal from wastewater by pistachio wood wastes-derived activated carbon prepared by chemical activation using a novel activating agent. *J. Environ. Manag.* **2018**, *223*, 1001–1009. [[CrossRef](#)]
50. Ouhammou, M.; Lahnine, L.; Mghazli, S.; Hidar, N.; Bouchdoug, M.; Jaouad, A.; Mandi, L.; Mahrouz, M. Valorisation of cellulosic waste basic cactus to prepare activated carbon. *J. Saudi Soc. Agric. Sci.* **2019**, *18*, 133–140. [[CrossRef](#)]
51. Björklund, K.; Li, L.Y. Adsorption of organic stormwater pollutants onto activated carbon from sewage sludge. *J. Environ. Manag.* **2017**, *197*, 490–497. [[CrossRef](#)] [[PubMed](#)]
52. Benstoem, F.; Becker, G.; Firk, J.; Kaless, M.; Wuest, D.; Pinnekamp, J.; Kruse, A. Elimination of micropollutants by activated carbon produced from fibers taken from wastewater screenings using hydrothermal carbonization. *J. Environ. Manag.* **2018**, *211*, 278–286. [[CrossRef](#)] [[PubMed](#)]
53. Pirsahab, M.; Mohamadi, S.; Rahmatabadi, S.; Hossini, H.; Motteran, F. Simultaneous wastewater treatment and biogas production using integrated anaerobic baffled reactor granular activated carbon from baker's yeast wastewater. *Environ. Technol.* **2018**, *39*, 2724–2735. [[CrossRef](#)] [[PubMed](#)]
54. Jahandar, L.M.; Atkinson, J.D.; Hashisho, Z.; Phillips, J.H.; Anderson, J.E.; Nichols, M. The role of beaded activated carbon's surface oxygen groups on irreversible adsorption of organic vapors. *J. Hazard. Mater.* **2016**, *317*, 284–294. [[CrossRef](#)] [[PubMed](#)]
55. Fu, Y.; Zhang, Y.; Li, G.; Zhang, J.; Guo, Y. NO removal activity and surface characterization of activated carbon with oxidation modification. *J. Energy Inst.* **2017**, *90*, 813–823. [[CrossRef](#)]
56. Ren, S.; Guo, F.; Yang, J.; Yao, L.; Zhao, Q.; Kong, M. Selection of carbon materials and modification methods in low-temperature sintering flue gas denitrification. *Chem. Eng. Res. Des.* **2017**, *126*, 278–285. [[CrossRef](#)]
57. Jie, W.; Lin, H.; Xue, H.; Ying, Z.; Wei, C. Physicochemical studies of adsorptive denitrogenation by oxidized activated carbons. *Ind. Eng. Chem. Res.* **2017**, *56*, 5033–5041.

58. Chong-jiu, L.; Zhao, R.; Meng-qi, P.; Liu, H.; Gang, Y.U.; Xia, D.S. Study on desulfurization and denitrification by modified activated carbon fibers with visible-light photocatalysis. *J. Fuel Chem. Technol.* **2015**, *43*, 1516–1522.
59. Arcibar-Orozco, J.A.; Acosta-Herrera, A.A.; Rangel-Mendez, J.R. Simultaneous desulfuration and denitrogenation of model diesel fuel by Fe-Mn microwave modified activated carbon: Iron crystalline habit influence on adsorption capacity. *J. Clean. Prod.* **2019**, *218*, 69–82. [[CrossRef](#)]
60. You, F.T.; Yu, G.W.; Xing, Z.J.; Li, J.; Xie, S.Y.; Li, C.X.; Wang, G.; Ren, H.Y.; Wang, Y. Enhancement of NO catalytic oxidation on activated carbon at room temperature by nitric acid hydrothermal treatment. *Appl. Surf. Sci.* **2019**, *471*, 633–644. [[CrossRef](#)]
61. Sun, X.; Sun, L.; Liu, Y.; Li, K.; Wang, C.; Song, X.; Ning, P. Research on reaction conditions and mechanism for simultaneous removal of NO and Hg⁰ over CuFe modified activated carbon at low temperature. *J. Energy Inst.* **2019**, *6*, 223–228.
62. Wei, Z.S.; Zeng, G.H.; Xie, Z.R.; Ma, C.Y.; Liu, X.H.; Sun, J.L.; Liu, L.H. Microwave catalytic NO_x and SO₂ removal using FeCu/zeolite as catalyst. *Fuel* **2011**, *90*, 1599–1603. [[CrossRef](#)]
63. Li, G.; Wang, B.; Sun, Q.; Xu, W.Q.; Ma, Z.; Wang, H.; Zhang, D.; Zhou, J. Novel synthesis of fly-ash-derived Cu-loaded SAPO-34 catalysts and their use in selective catalytic reduction of NO with NH₃. *Green Energy Environ.* **2019**, *32*, 234–239. [[CrossRef](#)]
64. Agote-Arán, M.; Lezcano-González, I.; Greenaway, A.G.; Hayama, S.; Díaz-Moreno, S.; Kroner, A.B.; Beale, A.M. Operando HERFD-XANES/XES studies reveal differences in the activity of Fe-species in MFI and CHA structures for the standard selective catalytic reduction of NO with NH₃. *Appl. Catal. A: Gen.* **2019**, *570*, 283–291. [[CrossRef](#)]
65. Chen, L.; Wang, X.; Cong, Q.; Ma, H.; Li, S.; Li, W. Design of a hierarchical Fe-ZSM-5@CeO₂ catalyst and the enhanced performances for the selective catalytic reduction of NO with NH₃. *Chem. Eng. J.* **2019**, *369*, 957–967. [[CrossRef](#)]
66. Baran, R.; Averseng, F.; Wierzbicki, D.; Chalupka, K.; Krafft, J.-M.; Grzybek, T.; Dzwigaj, S. Effect of postsynthesis preparation procedure on the state of copper in CuBEA zeolites and its catalytic properties in SCR of NO with NH₃. *Appl. Catal. A: Gen.* **2016**, *523*, 332–342. [[CrossRef](#)]
67. Ma, Y.; Li, J.; Liu, E.; Wan, J.; Hu, X.; Fan, J. High efficiency for H₂ evolution and NO removal over the Ag nanoparticles bridged g-C₃N₄ and WS₂ heterojunction photocatalysts. *Appl. Catal. B: Environ.* **2017**, *219*, 467–478. [[CrossRef](#)]
68. Imai, S.; Miura, H.; Shishido, T. Selective catalytic reduction of NO with CO and C₃H₆ over Rh/NbOPO₄. *Catal. Today* **2019**, *332*, 267–271. [[CrossRef](#)]
69. Xiao, P.; Davis, R.C.; Ouyang, X.; Li, J.; Thomas, A.; Scott, S.L.; Zhu, J. Mechanism of NO reduction by CO over Pt/SBA-15. *Catal. Commun.* **2014**, *50*, 69–72. [[CrossRef](#)]
70. Wang, L.; Cheng, X.; Wang, Z.; Ma, C.; Qin, Y. Investigation on Fe-Co binary metal oxides supported on activated semi-coke for NO reduction by CO. *Appl. Catal. B: Environ.* **2017**, *201*, 636–651. [[CrossRef](#)]
71. Chen, W.; Li, Z.; Hu, F.; Qin, L.; Han, J.; Wu, G. In-situ DRIFTS investigation on the selective catalytic reduction of NO with NH₃ over the sintered ore catalyst. *Appl. Surf. Sci.* **2018**, *439*, 75–81. [[CrossRef](#)]
72. Chen, Q.; Zheng, J.; Wen, L.; Yang, C.; Zhang, L. A multi-functional-group modified cellulose for enhanced heavy metal cadmium adsorption: Performance and quantum chemical mechanism. *Chemosphere* **2019**, *224*, 509–518. [[CrossRef](#)] [[PubMed](#)]
73. Wang, H.; Ning, P.; Zhang, Q.; Liu, X.; Zhang, T.; Fan, J.; Wang, J.; Long, K. Promotional mechanism of WO₃ over RuO₂-Fe₂O₃ catalyst for NH₃-SCO reaction. *Appl. Catal. A: Gen.* **2018**, *561*, 158–167. [[CrossRef](#)]
74. Ibusuki, T.; Takeuchi, K. Removal of low concentration nitrogen oxides through photoassisted heterogeneous catalysis. *J. Mol. Catal.* **1994**, *88*, 93–102. [[CrossRef](#)]
75. Huang, J.; Huang, H.; Liu, L.; Jiang, H. Revisit the effect of manganese oxidation state on activity in low-temperature NO-SCR. *Mol. Catal.* **2018**, *446*, 49–57. [[CrossRef](#)]
76. Jiang, L.; Liu, Q.; Ran, G.; Kong, M.; Ren, S.; Yang, J.; Li, J. V₂O₅-modified Mn-Ce/AC catalyst with high SO₂ tolerance for low-temperature NH₃-SCR of NO. *Chem. Eng. J.* **2019**, *370*, 810–821. [[CrossRef](#)]
77. Lin, F.; Shao, J.; Tang, H.; Li, Y.; Wang, Z.; Chen, G.; Yuan, D.; Cen, K. Enhancement of NO oxidation activity and SO₂ resistance over LaMnO₃+ δ perovskites catalysts with metal substitution and acid treatment. *Appl. Surf. Sci.* **2019**, *479*, 234–246. [[CrossRef](#)]

78. Salman, A.U.R.; Enger, B.C.; Auvray, X.; Lødeng, R.; Menon, M.; Waller, D.; Rønning, M. Catalytic oxidation of NO to NO₂ for nitric acid production over a Pt/Al₂O₃ catalyst. *Appl. Catal. A: Gen.* **2018**, *564*, 142–146. [[CrossRef](#)]
79. Jia, J.; Ran, R.; Guo, X.; Wu, X.; Chen, W.; Weng, D. Enhanced low-temperature NO oxidation by iron-modified MnO₂ catalysts. *Catal. Commun.* **2019**, *119*, 139–143. [[CrossRef](#)]
80. Yuan, P.; Egedy, A.; Miskolczi, N.; Shen, B.; Wang, J.; Zhou, W.; Pan, Y.; Zhang, H. Oxidation removal of NO by in situ Fenton system: Factors and optimization. *Fuel* **2018**, *233*, 519–528. [[CrossRef](#)]
81. Zhao, Y.; Hao, R.; Wang, T.; Yang, C. Follow-up research for integrative process of pre-oxidation and post-absorption cleaning flue gas: Absorption of NO₂, NO and SO₂. *Chem. Eng. J.* **2015**, *273*, 55–65. [[CrossRef](#)]
82. Guo, L.; Han, C.; Zhang, S.; Zhong, Q.; Ding, J.; Zhang, B.; Zeng, Y. Enhancement effects of O₂⁻ and OH radicals on NO_x removal in the presence of SO₂ by using an O₃/H₂O₂ AOP system with inadequate O₃ (O₃/NO molar ratio = 0.5). *Fuel* **2018**, *233*, 769–777. [[CrossRef](#)]
83. Fei, L.; Lin, Q.; Bi, X.; Chan, L.Y.; Chen, S.; Yan, X.; Liu, Y.; Wang, X.; Zhang, Y.; Cen, C. Effect of lightning activities on surface atmospheric NO, O₃ and submicron particles based on artificially triggered lightning technology: A case study. *Atmos. Pollut. Res.* **2019**, *10*, 105–110. [[CrossRef](#)]
84. Hultén, A.H.; Nilsson, P.; Samuelsson, M.; Ajdari, S.; Normann, F.; Andersson, K. First evaluation of a multicomponent flue gas cleaning concept using chlorine dioxide gas—Experiments on chemistry and process performance. *Fuel* **2017**, *210*, 885–891. [[CrossRef](#)]
85. Sun, W.Y.; Ding, S.L.; Zeng, S.S.; Su, S.J.; Jiang, W.J. Simultaneous absorption of NO_x and SO₂ from flue gas with pyrolusite slurry combined with gas-phase oxidation of NO using ozone. *J. Hazard. Mater.* **2011**, *192*, 124–130. [[CrossRef](#)] [[PubMed](#)]
86. Mok, Y.S.; LEE, H.J. Removal of sulfur dioxide and nitrogen oxides by using ozone injection and absorption-reduction technique. *Fuel Process. Technol.* **2006**, *87*, 591–597. [[CrossRef](#)]
87. Lin, F.; Wang, Z.; Ma, Q.; Yang, Y.; Whiddon, R.; Zhu, Y.; Cen, K. Catalytic deep oxidation of NO by ozone over MnO_x loaded spherical alumina catalyst. *Appl. Catal. B: Environ.* **2016**, *198*, 100–111. [[CrossRef](#)]
88. Han, C.; Zhang, S.; Guo, L.; Zeng, Y.; Li, X.; Shi, Z.; Zhang, Y.; Zhang, B.; Zhong, Q. Enhanced catalytic ozonation of NO over black-TiO₂ catalyst under inadequate ozone (O₃/NO molar ratio = 0.6). *Chem. Eng. Res. Des.* **2018**, *136*, 219–229. [[CrossRef](#)]
89. Hao, R.; Mao, X.; Wang, Z.; Zhao, Y.; Wang, T.; Sun, Z.; Yuan, B.; Li, Y. A novel method of ultraviolet/NaClO₂-NH₄OH for NO removal: Mechanism and kinetics. *J. Hazard. Mater.* **2019**, *368*, 234–242. [[CrossRef](#)]
90. Zhao, Y.; Guo, T.X.; Chen, Z.Y.; Du, Y.R. Simultaneous removal of SO₂ and NO using M/NaClO₂ complex absorbent. *Chem. Eng. J.* **2010**, *160*, 42–47. [[CrossRef](#)]
91. Deshwal, B.R.; Si, H.L.; Jung, J.H.; Shon, B.H.; Lee, H.K. Study on the removal of NO_x from simulated flue gas using acidic NaClO₂ solution. *J. Environ. Sci.* **2008**, *20*, 33–38. [[CrossRef](#)]
92. Hao, R.; Yang, S.; Bo, Y.; Yi, Z. Simultaneous desulfurization and denitrification through an integrative process utilizing NaClO₂/Na₂S₂O₈. *Fuel Process. Technol.* **2017**, *159*, 145–152. [[CrossRef](#)]
93. Yang, S.; Pan, X.; Han, Z.; Zheng, D.; Yu, J.; Xia, P.; Liu, B.; Yan, Z. Nitrogen Oxide Removal from Simulated Flue Gas by UV-Irradiated Sodium Chlorite Solution in a Bench-Scale Scrubbing Reactor. *Ind. Eng. Chem. Res.* **2017**, *56*, 3671–3678. [[CrossRef](#)]
94. Wang, W.; Guo, R.; Pan, W.; Hu, G. Low temperature catalytic oxidation of NO over different-shaped CeO₂. *J. Rare Earths* **2018**, *36*, 588–593. [[CrossRef](#)]
95. Zhao, S.; Wang, L.; Wang, Y.; Li, X. Hierarchically porous LaFeO₃ perovskite prepared from the pomelo peel bio-template for catalytic oxidation of NO. *J. Phys. Chem. Solids* **2018**, *116*, 43–49. [[CrossRef](#)]
96. Shang, H.; Li, Y.; Liu, J.; Tang, X.; Yang, J.; Li, J. CH₄/N₂ separation on methane molecules grade diameter channel molecular sieves with a CHA-type structure. *Chin. J. Chem. Eng.* **2018**, *1*, 102–110. [[CrossRef](#)]
97. Yamane, Y.; Tanaka, H.; Miyahara, M.T. In silico synthesis of carbon molecular sieves for high-performance air separation. *Carbon* **2019**, *141*, 626–634. [[CrossRef](#)]
98. Liu, X.; Jiang, S.; Li, H.; Yang, J.; Yang, Z.; Zhao, J.; Peng, H.; Shih, K. Elemental mercury oxidation over manganese oxide octahedral molecular sieve catalyst at low flue gas temperature. *Chem. Eng. J.* **2019**, *356*, 142–150. [[CrossRef](#)]

99. Geng, Q.; Wang, L.J.; Yang, C.; Zhang, H.Y.; Zhao, Y.R.; Fan, H.L.; Huo, C. Room-temperature hydrogen sulfide removal with zinc oxide nanoparticle/molecular sieve prepared by melt infiltration. *Fuel Process. Technol.* **2019**, *185*, 26–37. [[CrossRef](#)]
100. Dharmarathna, S.; King'onde, C.K.; Pahalagedara, L.; Kuo, C.H.; Zhang, Y.; Suib, S.L. Manganese octahedral molecular sieve (OMS-2) catalysts for selective aerobic oxidation of thiols to disulfides. *Appl. Catal. B: Environ.* **2014**, *147*, 124–131. [[CrossRef](#)]
101. Park, D.; Ju, Y.; Kim, J.H.; Ahn, H.; Lee, C.H. Equilibrium and kinetics of nitrous oxide, oxygen and nitrogen adsorption on activated carbon and carbon molecular sieve. *Sep. Purif. Technol.* **2019**, *223*, 63–80. [[CrossRef](#)]
102. Sarmah, B.; Srivastava, R. Selective two-step synthesis of 2,5-diformylfuran from monosaccharide, disaccharide, and polysaccharide using H-Beta and octahedral MnO₂ molecular sieves. *Mol. Catal.* **2019**, *462*, 92–103. [[CrossRef](#)]
103. Hamaguchi, T.; Tanaka, T.; Takahashi, N.; Tsukamoto, Y.; Takagi, N.; Shinjoh, H. Low-temperature NO-adsorption properties of manganese oxide octahedral molecular sieves with different potassium content. *Appl. Catal. B: Environ.* **2016**, *193*, 234–239. [[CrossRef](#)]
104. Tolaymat, T.; El Badawy, A.; Genaidy, A.; Abdelraheem, W.; Sequeira, R. Analysis of metallic and metal oxide nanomaterial environmental emissions. *J. Clean. Prod.* **2017**, *143*, 401–412. [[CrossRef](#)]
105. Jögi, I.; Erme, K.; Raud, J.; Laan, M. Oxidation of NO by ozone in the presence of TiO₂ catalyst. *Fuel* **2016**, *173*, 45–51. [[CrossRef](#)]
106. Wang, H.; Chen, H.; Wang, Y.; Lyu, Y.K. Performance and mechanism comparison of manganese oxides at different valence states for catalytic oxidation of NO. *Chem. Eng. J.* **2019**, *361*, 1161–1172. [[CrossRef](#)]
107. Ma, S.J.; Wang, X.W.; Chen, T.; Yuan, Z.H. Effect of surface morphology on catalytic activity for NO oxidation of SmMn₂O₅ nanocrystals. *Chem. Eng. J.* **2018**, *354*, 191–196. [[CrossRef](#)]
108. Cai, W.; Zhao, Y.; Chen, M.; Jiang, X.; Wang, H.; Ou, M.; Wan, S.; Zhong, Q. The formation of 3D spherical Cr-Ce mixed oxides with roughness surface and their enhanced low-temperature NO oxidation. *Chem. Eng. J.* **2017**, *333*, 414–422. [[CrossRef](#)]
109. Wang, Z.; Huang, Y.; Ho, W.; Cao, J.; Shen, Z.; Lee, S.C. Fabrication of Bi₂O₂CO₃/g-C₃N₄ heterojunctions for efficiently photocatalytic NO in air removal: In-situ self-sacrificial synthesis, characterizations and mechanistic study. *Appl. Catal. B: Environ.* **2016**, *199*, 123–133. [[CrossRef](#)]
110. Ângelo, J.; Andrade, L.; Madeira, L.M.; Mendes, A. An overview of photocatalysis phenomena applied to NO_x abatement. *J. Environ. Manag.* **2013**, *129*, 522–539. [[CrossRef](#)] [[PubMed](#)]
111. Duan, Y.; Luo, J.; Zhou, S.; Mao, X.; Shah, M.W.; Wang, F.; Chen, Z.; Wang, C. TiO₂-supported Ag nanoclusters with enhanced visible light activity for the photocatalytic removal of NO. *Appl. Catal. B: Environ.* **2018**, *234*, 206–212. [[CrossRef](#)]
112. He, D.; Li, Y.; Wang, I.; Wu, J.; Yang, Y.; An, Q. Carbon wrapped and doped TiO₂ mesoporous nanostructure with efficient visible-light photocatalysis for NO removal. *Appl. Surf. Sci.* **2017**, *391*, 318–325. [[CrossRef](#)]
113. Yuan, Y.; Zhang, J.; Li, H.; Li, Y.; Zhao, Y.; Zheng, C. Simultaneous removal of SO₂, NO and mercury using TiO₂-aluminum silicate fiber by photocatalysis. *Chem. Eng. J.* **2012**, *192*, 21–28. [[CrossRef](#)]
114. Jin, S.; Dong, G.; Luo, J.; Ma, F.; Wang, C. Improved photocatalytic NO removal activity of SrTiO₃ by using SrCO₃ as a new co-catalyst. *Appl. Catal. B: Environ.* **2018**, *227*, 24–34. [[CrossRef](#)]
115. Huy, T.H.; Bui, D.P.; Kang, F.; Wang, Y.F.; Liu, S.H.; Thi, C.M.; You, S.J.; Chang, G.M.; Pham, V.V. SnO₂/TiO₂ nanotube heterojunction: The first investigation of NO degradation by visible light-driven photocatalysis. *Chemosphere* **2019**, *215*, 323–332. [[CrossRef](#)] [[PubMed](#)]
116. Su, X.; Li, X.; Ma, L.; Fan, J. Formation and transformation of schwertmannite in the classic Fenton process. *J. Environ. Sci.* **2019**, *82*, 145–154. [[CrossRef](#)]
117. Zhang, Y.; Liang, J.; Zhou, W.; Xiao, N. Comparison of Fenton and bismuth ferrite Fenton-like pretreatments of sugarcane bagasse to enhance enzymatic saccharification. *Bioresour. Technol.* **2019**, *285*, 121343. [[CrossRef](#)]
118. Hao, R.; Mao, Y.; Mao, X.; Wang, Z.; Gong, Y.; Zhang, Z.; Zhao, Y. Cooperative removal of SO₂ and NO by using a method of UV-heat/H₂O₂ oxidation combined with NH₄OH-(NH₄)₂SO₃ dual-area absorption. *Chem. Eng. J.* **2019**, *365*, 282–290. [[CrossRef](#)]
119. Song, Z.; Wang, B.; Yu, J.; Ma, C.; Chen, T.; Yang, W.; Liu, S.; Sun, L. Effect of Ti doping on heterogeneous oxidation of NO over Fe₃O₄ (111) surface by H₂O₂: A density functional study. *Chem. Eng. J.* **2018**, *354*, 517–524. [[CrossRef](#)]

120. Wu, B.; Zhang, S.; He, S.; Xiong, Y. Follow-up mechanism study on NO oxidation with vaporized H₂O₂ catalyzed by Fe₂O₃ in a fixed-bed reactor. *Chem. Eng. J.* **2019**, *356*, 662–672. [[CrossRef](#)]
121. Wang, Y.; Liu, Y.; Liu, Y. Elimination of Nitric Oxide Using New Fenton Process Based on Synergistic Catalysis: Optimization and Mechanism. *Chem. Eng. J.* **2019**, *372*, 92–98. [[CrossRef](#)]
122. Yi, Z.; Wen, X.; Guo, T.; Zhou, J.; Fuproc, J.; Process, W. Desulfurization and denitrogenation from flue gas using Fenton reagent. *Fuel Process. Technol.* **2014**, *128*, 54–60.
123. Cheng, L.; Huang, J.; Ni, F. Generation kinetics of hydroxyl radicals by Fenton's reagent. *Tech. Equip. Environ. Pollut. Control* **2003**, *12*, 189–195.
124. Guo, R.T.; Pan, W.G.; Zhang, X.B.; Ren, J.X.; Qiang, J.; Xu, H.J.; Jiang, W. Removal of NO by using Fenton reagent solution in a lab-scale bubbling reactor. *Fuel* **2011**, *90*, 3295–3298. [[CrossRef](#)]
125. Cui, R.; Yang, B.; Li, S.; Wang, J.; Ma, S. Heterogeneous Fenton catalysts prepared from modified-fly ash for NO_x removal with H₂O₂. *Catal. Commun.* **2019**, *119*, 180–184. [[CrossRef](#)]
126. Zhao, Y.; Han, Y.; Wang, T.; Sun, Z.; Fang, C. Simultaneous removal of SO₂ and NO from flue gas using iron-containing polyoxometalates as heterogeneous catalyst in UV-Fenton-like process. *Fuel* **2019**, *250*, 42–51. [[CrossRef](#)]
127. Yuan, P.; Mei, X.; Shen, B.; Lu, F.; Zhou, W.; Si, M.; Chakraborty, S. Oxidation of NO by in situ Fenton reaction system with dual ions as reagents. *Chem. Eng. J.* **2018**, *351*, 660–667. [[CrossRef](#)]
128. Góra-Marek, K.; Brylewska, K.; Tarach, K.A.; Rutkowska, M.; Jabłońska, M.; Choi, M.; Chmielarz, L. IR studies of Fe modified ZSM-5 zeolites of diverse mesopore topologies in the terms of their catalytic performance in NH₃-SCR and NH₃-SCO processes. *Appl. Catal. B: Environ.* **2015**, *179*, 589–598. [[CrossRef](#)]
129. Schiavoni, M.; Campisi, S.; Gervasini, A. Effect of Cu deposition method on silico aluminophosphate catalysts in NH₃-SCR and NH₃-SCO reactions. *Appl. Catal. A: Gen.* **2017**, *543*, 162–172. [[CrossRef](#)]
130. Shi-Gu, Q.; Wang, Y.; Li, X. Effect of praseodymium substitution on La_{1-x}Pr_xMnO₃ (x = 0–0.4) perovskites and catalytic activity for NO oxidation. *J. Phys. Chem. Solids* **2019**, *133*, 52–58.
131. Wang, H.; Xu, R.; Jin, Y.; Zhang, R. Zeolite structure effects on Cu active center, SCR performance and stability of Cu-zeolite catalysts. *Catal. Today* **2019**, *327*, 295–307. [[CrossRef](#)]
132. Yu, S.; Lu, Y.; Gao, F.; Dong, L. Study on the Crystal Plane Effect of CuO/TiO₂ Catalysts in NH₃-SCR Reaction. *Catal. Today* **2019**, *327*, 235–245. [[CrossRef](#)]
133. Ling, L.; Cao, Y.; Zhao, Z.; Liu, P.; Wang, B.; Zhang, R.; Li, D. Density functional theory calculations and analysis for the reduction of NO by H₂ on Pd₆/TiO₂. *Comput. Mater. Sci.* **2018**, *149*, 182–190. [[CrossRef](#)]
134. Jung, Y.; Pyo, Y.D.; Jang, J.; Kim, G.C.; Cho, C.P.; Yang, C. NO, NO₂ and N₂O emissions over a SCR using DOC and DPF systems with Pt reduction. *Chem. Eng. J.* **2019**, *369*, 1059–1067. [[CrossRef](#)]
135. Locci, C.; Vervisch, L.; Farcy, B.; Domingo, P.; Perret, N. Selective Non-catalytic Reduction (SNCR) of Nitrogen Oxide Emissions: A Perspective from Numerical Modeling. *Flow Turbul. Combust.* **2018**, *100*, 301–340. [[CrossRef](#)]
136. Hao, J.; Yu, W.; Lu, P.; Zhang, Y.; Zhu, X. The effects of Na/K additives and flyash on NO reduction in a SNCR process. *Chemosphere* **2015**, *122*, 213–218. [[CrossRef](#)] [[PubMed](#)]
137. Fu, S.L.; Song, Q.; Yao, Q. Influence of CaO on urea pyrolysis in the selective non-catalytic reduction deNO_x process. *J. Anal. Appl. Pyrolysis* **2017**, *126*, 397–404. [[CrossRef](#)]
138. Chen, H.; Chen, D.Z.; Fan, S.; Hong, L.; Wang, D. SNCR De-NO_x within a moderate temperature range using urea-spiked hydrazine hydrate as reductant. *Chemosphere* **2016**, *161*, 208–218. [[CrossRef](#)]
139. Kang, Z.; Yuan, Q.; Zhao, L.; Dai, Y.; Sun, B.; Wang, T. Study of the performance, simplification and characteristics of SNCR de-NO_x in large-scale cyclone separator. *Appl. Therm. Eng.* **2017**, *123*, 635–645. [[CrossRef](#)]
140. Fu, S.L.; Song, Q.; Yao, Q. Mechanism study on the adsorption and reactions of NH₃, NO, and O₂ on the CaO surface in the SNCR deNO_x process. *Chem. Eng. J.* **2016**, *285*, 137–143. [[CrossRef](#)]
141. Fu, S.L.; Song, Q.; Yao, Q. Study on the catalysis of CaCO₃ in the SNCR deNO_x process for cement kilns. *Chem. Eng. J.* **2015**, *262*, 9–17. [[CrossRef](#)]
142. Tan, L.; Guo, Y.; Liu, Z.; Feng, P.; Li, Z. An investigation on the catalytic characteristic of NO_x reduction in SCR systems. *J. Taiwan Inst. Chem. Eng.* **2019**, *65*, 236–246.
143. Odenbrand, C.U.I. CaSO₄ deactivated V₂O₅-WO₃/TiO₂ SCR catalyst for a diesel power plant. Characterization and simulation of the kinetics of the SCR reactions. *Appl. Catal. B: Environ.* **2018**, *234*, 365–377. [[CrossRef](#)]

144. Lu, J.; Zhou, Z.; Zhang, H.; Yang, Z. Influenced factors study and evaluation for SO₂/SO₃ conversion rate in SCR process. *Fuel* **2019**, *245*, 528–533. [[CrossRef](#)]
145. Yu, S.; Lu, Y.; Cao, Y.; Wang, J.; Sun, B.; Gao, F.; Tang, C.; Dong, L. Composite catalytic systems: A strategy for developing the low temperature NH₃-SCR catalysts with satisfactory SO₂ and H₂O tolerance. *Catal. Today* **2019**, *327*, 235–245. [[CrossRef](#)]
146. Gao, F.; Tang, X.; Yi, H.; Zhao, S.; Wang, J.; Gu, T. Improvement of activity, selectivity and H₂O&SO₂-tolerance of micro-mesoporous CrMn₂O₄ spinel catalyst for low-temperature NH₃-SCR of NO_x. *Appl. Surf. Sci.* **2019**, *466*, 411–424.
147. Guo, M.; Liu, Q.; Zhao, P.; Han, J.; Li, X.; Ha, Y.; Fu, Z.; Song, C.; Ji, N.; Liu, C.; et al. Promotional effect of SO₂ on Cr₂O₃ catalysts for the marine NH₃-SCR reaction. *Chem. Eng. J.* **2019**, *361*, 830–838. [[CrossRef](#)]
148. Niu, C.; Niu, J.; Wang, S.; Wang, Z.; Dong, S.; Fan, H.; Hong, Y.; Liu, D. Synergistic effect in one-stage dielectric barrier discharge plasma and Ag/Al₂O₃ catalytic systems on C₂H₂-SCR of NO_x. *Catal. Commun.* **2019**, *123*, 49–53. [[CrossRef](#)]
149. Sun, X.; Guo, R.T.; Liu, S.W.; Liu, J.; Pan, W.G.; Shi, X.; Qin, H.; Wang, Z.Y.; Qiu, Z.Z.; Liu, X.Y. The promoted performance of CeO₂ catalyst for NH₃-SCR reaction by NH₃ treatment. *Appl. Surf. Sci.* **2018**, *462*, 187–193. [[CrossRef](#)]
150. Li, X.; Li, X.; Yang, R.T.; Mo, J.; Li, J.; Hao, J. The poisoning effects of calcium on V₂O₅-WO₃/TiO₂ catalyst for the SCR reaction: Comparison of different forms of calcium. *Mol. Catal.* **2017**, *434*, 16–24. [[CrossRef](#)]
151. Jung, Y.; Shin, Y.J.; Pyo, Y.D.; Cho, C.P.; Jang, J.; Kim, G. NO_x and N₂O emissions over a Urea-SCR system containing both V₂O₅-WO₃/TiO₂ and Cu-zeolite catalysts in a diesel engine. *Chem. Eng. J.* **2017**, *326*, 853–862. [[CrossRef](#)]
152. Liang, Q.M.; Li, J.; He, H.; Liang, W.J.; Zhang, T.J.; Fan, X. Effects of SO₂ on the low temperature selective catalytic reduction of NO by NH₃ over CeO₂-V₂O₅-WO₃/TiO₂ catalysts. *Front. Environ. Sci. Eng.* **2017**, *11*, 4. [[CrossRef](#)]
153. Li, P.; Liu, Q.; Liu, Z. Behaviors of NH₄HSO₄ in SCR of NO by NH₃ over different cokes. *Chem. Eng. J.* **2012**, *181*, 169–173. [[CrossRef](#)]
154. Ye, D.; Qu, R.; Zheng, C.; Cen, K.; Gao, X. Mechanistic investigation of enhanced reactivity of NH₄HSO₄ and NO on Nb- and Sb-doped VW/Ti SCR catalysts. *Appl. Catal. A: Gen.* **2018**, *549*, 310–319. [[CrossRef](#)]
155. Zhao, X.; Mao, L.; Dong, G. Mn-Ce-V-WO_x/TiO₂ SCR Catalysts: Catalytic Activity, Stability and Interaction among Catalytic Oxides. *Catalysts* **2018**, *8*, 76. [[CrossRef](#)]
156. Tarot, M.L.; Barreau, M.; Duprez, D.; Lauga, V.; Iojoiu, E.; Courtois, X.; Can, F. Influence of the Sodium Impregnation Solvent on the Deactivation of Cu/FER-Exchanged Zeolites Dedicated to the SCR of NO_x with NH₃. *Catalysts* **2018**, *8*, 3. [[CrossRef](#)]
157. Dong, L.; Fan, Y.; Ling, W.; Yang, C.; Huang, B. Effect of Ce/Y Addition on Low-Temperature SCR Activity and SO₂ and H₂O Resistance of MnO_x/ZrO₂/MWCNTs Catalysts. *Catalysts* **2017**, *7*, 181. [[CrossRef](#)]
158. Shi, C.; Chang, H.; Wang, C.; Zhang, T.; Peng, Y.; Li, M.; Wang, Y.; Li, J. Improved Activity and H₂O Resistance of Cu-Modified MnO₂ Catalysts for NO Oxidation. *Ind. Eng. Chem. Res.* **2018**, *57*, 920–926. [[CrossRef](#)]
159. Wang, C.; Yu, F.; Zhu, M.; Wang, X.; Dan, J.; Zhang, J.; Cao, P.; Dai, B. Microspherical MnO₂-CeO₂-Al₂O₃ mixed oxide for monolithic honeycomb catalyst and application in selective catalytic reduction of NO_x with NH₃ at 50–150 °C. *Chem. Eng. J.* **2018**, *346*, 182–192. [[CrossRef](#)]
160. Gao, C.; Shi, J.-W.; Fan, Z.; Gao, G.; Niu, C. Sulfur and Water Resistance of Mn-Based Catalysts for Low-Temperature Selective Catalytic Reduction of NO_x: A Review. *Catalysts* **2018**, *8*, 11. [[CrossRef](#)]
161. Zhang, K.; Yu, F.; Zhu, M.; Dan, J.; Wang, X.; Zhang, J.; Dai, B. Enhanced Low Temperature NO Reduction Performance via MnO_x-Fe₂O₃/Vermiculite Monolithic Honeycomb Catalysts. *Catalysts* **2018**, *8*, 100. [[CrossRef](#)]
162. Yu, T.; Hao, T.; Fan, D.; Wang, J.; Shen, M.; Li, W. Recent NH₃-SCR mechanism research over Cu/SAPO-34 catalyst. *J. Phys. Chem. C* **2014**, *118*, 6565–6575. [[CrossRef](#)]
163. Woo, J.; Leistner, K.; Bernin, D.; Ahari, H.; Shost, M.; Zammit, M.; Olsson, L. Effect of various structure directing agents (SDAs) on low-temperature deactivation of Cu/SAPO-34 during NH₃-SCR reaction. *Catal. Sci. Technol.* **2018**, *8*, 3–4. [[CrossRef](#)]
164. Ryu, T.; Kim, H.; Hong, S.B. Nature of active sites in Cu-LTA NH₃-SCR catalysts: A comparative study with Cu-SSZ-13. *Appl. Catal. B: Environ.* **2019**, *245*, 513–521. [[CrossRef](#)]

165. Campisi, S.; Galloni, M.G.; Bossola, F.; Gervasini, A. Comparative performance of copper and iron functionalized hydroxyapatite catalysts in NH₃-SCR. *Catal. Commun.* **2019**, *123*, 79–85. [[CrossRef](#)]
166. Yang, Y.; Liu, J.; Liu, F.; Wang, Z.; Ding, J.; Huang, H. Reaction mechanism for NH₃-SCR of NO_x over CuMn₂O₄ catalyst. *Chem. Eng. J.* **2019**, *361*, 578–587. [[CrossRef](#)]
167. Wu, X.; Wang, R.; Du, Y.; Zou, C.; Meng, H.; Xie, X. Performance enhancement of NH₃-SCR via employing hydrotalcite-like precursor to induce the decoration of NiO by TiO₂ phase. *Mol. Catal.* **2019**, *467*, 150–160. [[CrossRef](#)]
168. Wu, W.; Zeng, Z.; Lu, P.; Xing, Y.; Wei, J.; Yue, H.; Li, R. Simultaneous oxidation of Hg⁰ and NH₃-SCR of NO by nanophase Ce_xZr_yMn_zO₂ at low temperature: The interaction and mechanism. *Environ. Sci. Pollut. Res.* **2018**, *25*, 14471–14485. [[CrossRef](#)]
169. Xu, H.; Zan, Q.; Zong, C.; Quan, F.; Jian, M.; Yan, N. Catalytic oxidation and adsorption of Hg⁰ over low-temperature NH₃-SCR LaMnO₃ perovskite oxide from flue gas. *Appl. Catal. B Environ.* **2016**, *186*, 30–40. [[CrossRef](#)]
170. Tian, J.; Wang, C.; Yu, F.; Zhou, X.; Zhang, J.; Yang, S.; Dan, J.; Cao, P.; Dai, B.; Wang, Q.; et al. Mn-Ce-Fe-Al mixed oxide nanoparticles via a high shear mixer facilitated coprecipitation method for low temperature selective catalytic reduction of NO with NH₃. *Appl. Catal. A: Gen.* **2019**, *586*, 117237. [[CrossRef](#)]
171. Wang, C.; Yu, F.; Zhu, M.Y.; Tang, C.J.; Dong, L.; Dai, B. Both powdered and performed of MnO_x-CeO₂-Al₂O₃ catalysts synthesized by self-propagating high-temperature synthesis for the selective catalytic reduction of NO_x with NH₃. *ACS Omega* **2018**, *3*, 5692–5703. [[CrossRef](#)] [[PubMed](#)]
172. Wang, C.; Xia, W.; Zhao, Y. New insight into hydroxyl-mediated NH₃ formation on the Rh-CeO₂ catalyst surface during catalytic reduction of NO by CO. *Chin. J. Catal.* **2017**, *38*, 1399–1405. [[CrossRef](#)]
173. Zhang, S.; Zhao, Y.; Yang, J.; Zhang, J.; Zheng, C. Fe-modified MnO_x/TiO₂ as the SCR catalyst for simultaneous removal of NO and mercury from coal combustion flue gas. *Chem. Eng. J.* **2018**, *348*, 618–629. [[CrossRef](#)]
174. Wang, C.; Yu, F.; Zhu, M.; Shi, Y.; Dan, J.; Lv, Y.; Guo, X.; Dai, B. Up-scaled flash nano-precipitation production route to develop a MnO_x-CeO₂-Al₂O₃ catalyst with enhanced activity and H₂O resistant performance for NO_x selective catalytic reduction with NH₃. *Chem. Eng. Res. Des.* **2018**, *134*, 476–486. [[CrossRef](#)]
175. Xiang, J.; Wang, L.; Cao, F.; Qian, K.; Su, S.; Hu, S.; Wang, Y.; Liu, L. Adsorption properties of NO and NH₃ over MnO_x based catalyst supported on γ-Al₂O₃. *Chem. Eng. J.* **2016**, *302*, 570–576. [[CrossRef](#)]
176. Wang, X.; Li, X.; Zhao, Q.; Sun, W.; Tade, M.; Liu, S. Improved activity of W-modified MnO_x-TiO₂ catalysts for the selective catalytic reduction of NO with NH₃. *Chem. Eng. J.* **2016**, *288*, 216–222. [[CrossRef](#)]
177. Zhang, P.; Pan, W.G.; Guo, R.T.; Zhu, X.B.; Liu, J.; Qin, L.; She, X.L. The Mo modified Ce/TiO₂ catalyst for simultaneous Hg⁰ oxidation and NO reduction. *J. Energy Inst.* **2018**, *44*, 224–254. [[CrossRef](#)]
178. Zhao, D.; Wang, C.; Yu, F.; Shi, Y.; Cao, P.; Dan, J.; Chen, K.; Lv, Y.; Guo, X.; Dai, B. Enhanced Oxygen Vacancies in a Two-Dimensional MnAl-Layered Double Oxide Prepared via Flash Nanoprecipitation Offers High Selective Catalytic Reduction of NO_x with NH₃. *Nanomaterials* **2018**, *8*, 620. [[CrossRef](#)]
179. Wang, C.; Yu, F.; Zhu, M.; Tang, C.; Zhang, K.; Zhao, D.; Dong, L.; Dai, B. Highly selective catalytic reduction of NO_x by MnO_x-CeO₂-Al₂O₃ catalysts prepared by self-propagating high-temperature synthesis. *J. Environ. Sci.* **2019**, *75*, 124–135. [[CrossRef](#)]
180. Liu, Z.; Liu, Y.; Yuan, L.; Hang, S.; Ma, L. WO₃ promoted Mn-Zr mixed oxide catalyst for the selective catalytic reduction of NO_x with NH₃. *Acs Appl Mater. Interfaces* **2016**, *283*, 1044–1050.
181. Shin, B.; Chun, H.H.; Cha, J.S.; Shin, M.C.; Lee, H. Physico-Chemical Property and Catalytic Activity of a CeO₂-Doped MnO(x)-TiO₂ Catalyst with SO₂ Resistance for Low-Temperature NH₃-SCR of NO(x). *J. Nanosci. Nanotechnol.* **2016**, *16*, 4370. [[CrossRef](#)] [[PubMed](#)]
182. Gao, F.; Tang, X.; Yi, H.; Li, J.; Zhao, S.; Wang, J.; Chao, C.; Li, C. Promotional mechanisms of activity and SO₂ tolerance of Co- or Ni-doped MnO_x-CeO₂ catalysts for SCR of NO_x with NH₃ at low temperature. *Chem. Eng. J.* **2017**, *317*, 20–31. [[CrossRef](#)]
183. Cao, F.; Su, S.; Xiang, J.; Wang, P.Y.; Hu, S.; Sun, L.S.; Zhang, A.C. The activity and mechanism study of Fe-Mn-Ce/gamma-Al₂O₃ catalyst for low temperature selective catalytic reduction of NO with NH₃. *Fuel* **2015**, *139*, 232–239. [[CrossRef](#)]
184. Zhang, Q.; Qiu, C.; Xu, H.; Tao, L.; Lin, Z.; Gong, M.; Chen, Y. Low-temperature selective catalytic reduction of NO with NH₃ over monolith catalyst of MnO_x/CeO₂-ZrO₂-Al₂O₃. *Catal. Today* **2012**, *175*, 171–176. [[CrossRef](#)]

185. Tian, J.; Zhang, K.; Wang, W.; Wang, F.; Dan, J.; Yang, S.; Zhang, J.; Dai, B.; Yu, F. Enhanced selective catalytic reduction of NO with NH₃ via porous micro-spherical aggregates of Mn–Ce–Fe–Ti mixed oxide nanoparticles. *Green Energy Environ.* **2019**, *4*, 311–321. [[CrossRef](#)]
186. Cheng, X.; Cheng, Y.; Wang, Z.; Ma, C. Comparative study of coal based catalysts for NO adsorption and NO reduction by CO. *Fuel* **2018**, *214*, 230–241. [[CrossRef](#)]
187. Shen, B.; Zhu, S.; Zhang, X.; Chi, G.; Patel, D.; Si, M.; Wu, C. Simultaneous removal of NO and Hg⁰ using Fe and Co co-doped Mn-Ce/TiO₂ catalysts. *Fuel* **2018**, *224*, 241–249. [[CrossRef](#)]
188. Singh, S.; Bhatia, D. Modeling the role of CO and C₃H₆ in NO_x reduction on a Cu-CHA SCR catalyst. *Chem. Eng. J.* **2018**. [[CrossRef](#)]
189. Zheng, Y.; Harold, M.P.; Luss, D. Effects of CO, H₂ and C₃H₆ on Cu-SSZ-13 catalyzed NH₃-SCR. *Catal. Today* **2016**, *264*, 44–54. [[CrossRef](#)]
190. Liu, T.; Qian, J.; Yao, Y.; Shi, Z.; Han, L.; Liang, C.; Li, B.; Dong, L.; Fan, M.; Zhang, L. Research on SCR of NO with CO over the Cu_{0.1}La_{0.1}Ce_{0.8}O mixed-oxide catalysts: Effect of the grinding. *Mol. Catal.* **2017**, *430*, 43–53. [[CrossRef](#)]
191. Boningari, T.; Pavani, S.M.; Ettireddy, P.R.; Chuang, S.S.C.; Smirniotis, P.G. Mechanistic investigations on NO reduction with CO over Mn/TiO₂ catalyst at low temperatures. *Mol. Catal.* **2018**, *451*, 33–42. [[CrossRef](#)]
192. Panahi, P.N.; Salari, D.; Niaei, A.; Mousavi, S.M. NO reduction over nanostructure M-Cu/ZSM-5 (M: Cr, Mn, Co and Fe) bimetallic catalysts and optimization of catalyst preparation by RSM. *J. Ind. Eng. Chem.* **2013**, *19*, 1793–1799. [[CrossRef](#)]
193. Yang, D.; Fan, X.; Zhao, D.; An, Y.; Hu, Y.; Luo, Z. Sc₂CO₂ and Mn-doped Sc₂CO₂ as gas sensor materials to NO and CO: A first-principles study. *Phys. E: Low-Dimens. Syst. Nanostruct.* **2019**, *111*, 84–90. [[CrossRef](#)]
194. Chen, X.; Lyu, Y.; Nwabara, U.; Schwank, J.W. Reactivity study of CO+NO reaction over Pd/Al₂O₃ and Pd/CeZrO₂ catalysts. *Catal. Today* **2019**, *323*, 148–158. [[CrossRef](#)]
195. Cheng, G.; Tan, X.; Song, X.; Chen, X.; Dai, W.; Yuan, R.; Fu, X. Visible light assisted thermocatalytic reaction of CO + NO over Pd/LaFeO₃. *Appl. Catal. B: Environ.* **2019**, *251*, 130–142. [[CrossRef](#)]
196. Lopes, D.; Zotin, F.; Palacio, L.A. Copper-nickel catalysts from hydrotalcite precursors: The performance in NO reduction by CO. *Appl. Catal. B: Environ.* **2018**, *237*, 327–338. [[CrossRef](#)]
197. Bánsági, T.; Zakar, T.S.; Solymosi, F. An FTIR study on the formation of NCO surface complexes over Rh/CeO₂. *Appl. Catal. B: Environ.* **2006**, *66*, 147–150. [[CrossRef](#)]
198. Wang, L.; Cheng, X.; Wang, Z.; Huang, H.; Ma, C.; Qin, Y. Effect of the NO + CO reaction on the consumption of carbon supports: An in situ TG-FTIR analysis. *Chem. Eng. J.* **2018**, *352*, 90–102. [[CrossRef](#)]
199. Yamashita, S.; Yamamoto, Y.; Kawabata, H.; Niwa, Y.; Katayama, M.; Inada, Y. Dynamic chemical state conversion of nickel species supported on silica under CO–NO reaction conditions. *Catal. Today* **2018**, *303*, 33–39. [[CrossRef](#)]
200. Yao, X.; Li, L.; Zou, W.; Yu, S.; An, J.; Li, H.; Yang, F.; Dong, L. Preparation, characterization, and catalytic performance of high efficient CeO₂-MnO_x-Al₂O₃ catalysts for NO elimination. *Chin. J. Catal.* **2016**, *37*, 1369–1380. [[CrossRef](#)]
201. Jin, Q.; Shen, Y.; Sui, G.; Tao, X.; Pan, Y.; Zhu, S. Synergistic catalytic removals of NO, CO and HC over CeO₂ modified Mn-Mo-W-Ox/TiO₂-SiO₂ catalyst. *J. Rare Earths* **2018**, *36*, 148–155. [[CrossRef](#)]
202. Xu, G.; Ma, J.; Wang, L.; Xie, W.; Liu, J.; Yu, Y.; He, H. Insight into the origin of sulfur tolerance of Ag/Al₂O₃ in the H₂-C₃H₆-SCR of NO_x. *Appl. Catal. B: Environ.* **2019**, *244*, 909–918. [[CrossRef](#)]
203. Thomas, C. On an additional promoting role of hydrogen in the H₂-assisted C₃H₆-SCR of NO_x on Ag/Al₂O₃: A lowering of the temperature of formation–decomposition of the organo-NO_x intermediates? *Appl. Catal. B: Environ.* **2015**, *162*, 454–462. [[CrossRef](#)]
204. Xu, G.; Ma, J.; He, G.; Yu, Y.; He, H. An alumina-supported silver catalyst with high water tolerance for H₂ assisted C₃H₆-SCR of NO_x. *Appl. Catal. B: Environ.* **2017**, *207*, 60–71. [[CrossRef](#)]
205. Chaieb, T.; Delannoy, L.; Costentin, G.; Louis, C.; Casale, S.; Chantray, R.L.; Li, Z.Y.; Thomas, C. Insights into the influence of the Ag loading on Al₂O₃ in the H₂-assisted C₃H₆-SCR of NO_x. *Appl. Catal. B: Environ.* **2014**, *156*, 192–201. [[CrossRef](#)]
206. Yang, X.; Su, Y.X.; Qian, W.Y.; Yuan, M.H.; Zhou, H.; Deng, W.Y.; Zhao, B.T. Experimental study on selective catalytic reduction of NO by C₃H₆ over Fe-Ag/Al₂O₃ catalysts. *J. Fuel Chem. Technol.* **2017**, *45*, 1365–1375. [[CrossRef](#)]

207. Wang, X.; Wang, X.; Yu, H.; Wang, X. The functions of Pt located at different positions of HZSM-5 in H₂-SCR. *Chem. Eng. J.* **2019**, *355*, 470–477. [[CrossRef](#)]
208. Xue, Y.; Sun, W.; Wang, Q.; Cao, L.; Yang, J. Sparsely loaded Pt/MIL-96(Al) MOFs catalyst with enhanced activity for H₂-SCR in a gas diffusion reactor under 80 °C. *Chem. Eng. J.* **2018**, *335*, 612–620. [[CrossRef](#)]
209. Zhang, X.; Wang, X.; Zhao, X.; Xu, Y.; Liu, Y.; Yu, Q. Promotion effect of tungsten on the activity of Pt/HZSM-5 for H₂-SCR. *Chem. Eng. J.* **2015**, *260*, 419–426. [[CrossRef](#)]
210. Väliheikki, A.; Petalidou, K.C.; Kalamaras, C.M.; Kolli, T.; Huuhtanen, M.; Maunula, T.; Keiski, R.L.; Efstathiou, A.M. Selective catalytic reduction of NO_x by hydrogen (H₂-SCR) on WO_x-promoted CeZr1-zO₂ solids. *Appl. Catal. B: Environ.* **2014**, *156*, 72–83. [[CrossRef](#)]
211. Yang, S.; Wang, X.; Chu, W.; Song, Z.; Zhao, S. An investigation of the surface intermediates of H₂-SCR of NO_x over Pt/H-FER. *Appl. Catal. B: Environ.* **2011**, *107*, 380–385. [[CrossRef](#)]
212. Huai, L.Y.; He, C.Z.; Wang, H.; Wen, H.; Yi, W.C.; Liu, J.Y. NO dissociation and reduction by H₂ on Pd(1 1 1): A first-principles study. *J. Catal.* **2015**, *322*, 73–83. [[CrossRef](#)]
213. Liu, G.; Cui, Y.; Ji, J.; Shen, D.; Wang, Q.; Li, C.; Luo, K.H. A technical method to improve NO_x/NH₃ mixing ratio in SCR system and its engineering applications. *J. Energy Inst.* **2018**, *43*, 243–249. [[CrossRef](#)]
214. Kikugawa, M.; Yamazaki, K.; Kato, A.; Uyama, T.; Takahashi, N.; Shinjoh, H. Silver sulfate catalyst for soot oxidation with high resistance to sulfur poisoning. *Appl. Catal. A: Gen.* **2019**, *576*, 32–38. [[CrossRef](#)]
215. Tian, Y.; Yang, J.; Liu, L.; Liu, Q.; Kong, B.; Lin, F.; Kong, M.; Hu, G. Insight into regeneration mechanism with sulfuric acid for arsenic poisoned commercial SCR catalyst. *J. Energy Inst.* **2019**, *76*, 214–223. [[CrossRef](#)]
216. Wang, A.; Wang, Y.; Walter, E.D.; Washton, N.M.; Guo, Y.; Lu, G.; Peden, C.H.F.; Gao, F. NH₃-SCR on Cu, Fe and Cu+Fe exchanged beta and SSZ-13 catalysts: Hydrothermal aging and propylene poisoning effects. *Catal. Today* **2019**, *320*, 91–99. [[CrossRef](#)]
217. Hammershøi, P.S.; Jensen, A.D.; Janssens, T.V.W. Impact of SO₂-poisoning over the lifetime of a Cu-CHA catalyst for NH₃-SCR. *Appl. Catal. B: Environ.* **2018**, *238*, 104–110. [[CrossRef](#)]
218. Li, H.; Wang, S.; Wang, X.; Hu, J. Activity of CuCl₂-modified cobalt catalyst supported on Ti-Ce composite for simultaneous catalytic oxidation of Hg⁰ and NO in a simulated pre-sco process. *Chem. Eng. J.* **2017**, *316*, 1103–1113. [[CrossRef](#)]
219. Salazar, M.; Hoffmann, S.; Singer, V.; Becker, R.; Grünert, W. Hybrid catalysts for the selective catalytic reduction (SCR) of NO by NH₃. On the role of fast SCR in the reaction network. *Appl. Catal. B: Environ.* **2016**, *199*, 433–438. [[CrossRef](#)]
220. Han, S.; Cheng, J.; Ye, Q.; Cheng, S.; Kang, T.; Dai, H. Ce doping to Cu-SAPO-18: Enhanced catalytic performance for the NH₃-SCR of NO in simulated diesel exhaust. *Microporous Mesoporous Mater.* **2019**, *276*, 133–146. [[CrossRef](#)]
221. Xu, Y.; Wu, X.; Lin, Q.; Hu, J.; Ran, R.; Weng, D. SO₂ promoted V₂O₅-MoO₃/TiO₂ catalyst for NH₃-SCR of NO_x at low temperatures. *Appl. Catal. A: Gen.* **2019**, *570*, 42–50. [[CrossRef](#)]
222. Langmuir, I. Oscillations in Ionized Gases. *Proc. Natl. Acad. Sci. USA* **1928**, *14*, 627–637. [[CrossRef](#)] [[PubMed](#)]
223. Shahmansouri, M.; Misra, A.P. Surface plasmon oscillations in a semi-bounded semiconductor plasma. *Plasma Sci. Technol.* **2018**, *20*, 025001. [[CrossRef](#)]
224. Parastaev, A.; Hoeben, W.F.L.M.; van Heesch, B.E.J.M.; Kosinov, N.; Hensen, E.J.M. Temperature-programmed plasma surface reaction: An approach to determine plasma-catalytic performance. *Appl. Catal. B: Environ.* **2018**, *239*, 168–177. [[CrossRef](#)]
225. Shumyantseva, V.V.; Bulko, T.V.; Sigolaeva, L.V.; Kuzikov, A.V.; Pogodin, P.V.; Archakov, A.I. Molecular imprinting coupled with electrochemical analysis for plasma samples classification in acute myocardial infarction diagnostic. *Biosens. Bioelectron.* **2018**, *99*, 216–222. [[CrossRef](#)] [[PubMed](#)]
226. Shabbir, A.; Hornung, G.; Noterdaeme, J.-M.; Verdoolaege, G. Classification of ELM types in Joint European Torus based on global plasma parameters using discriminant analysis. *Fusion Eng. Des.* **2017**, *123*, 717–721. [[CrossRef](#)]
227. Gott, Y.V. Ion thermal conductivity in a tokamak plasma for the nonneoclassical distribution function (Review Paper). *Plasma Phys. Rep.* **1995**, *21*, 621–633.
228. Capitelli, M.; Capitelli, F.; Eletskii, A. Non-equilibrium and equilibrium problems in laser-induced plasmas. *Spectrochim. Acta Part. B At. Spectrosc.* **2000**, *55*, 559–574. [[CrossRef](#)]

229. Capitelli, M.; Armenise, I.; Bruno, D.; Cacciatore, M.; Celiberto, R.; Colonna, G.; Pascale, O.D.; Diomede, P.; Esposito, F.; Gorse, C. Non-equilibrium plasma kinetics: A state-to-state approach. *Plasma Sources Sci. Technol.* **2007**, *16*, S30–S44. [[CrossRef](#)]
230. Lourek, I.; Tribeche, M. Dust charging current in non equilibrium dusty plasma in the context of Kaniadakis generalization. *Phys. A: Stat. Mech. Appl.* **2019**, *517*, 522–529. [[CrossRef](#)]
231. Brzhozovskii, B.; Brovkova, M.; Gestrin, S.; Martynov, V.; Zinina, E. The effect of a combined low-pressure gas discharge on metal surfaces. *J. Phys. D Appl. Phys.* **2018**, *51*, 145204. [[CrossRef](#)]
232. Li, Y.; Wang, W.; Wang, F.; Di, L.; Yang, S.; Zhu, S.; Yao, Y.; Dai, B.; Ma, C.; Yu, F. Enhanced photocatalytic degradation of organic dyes via defect-rich TiO₂ prepared by dielectric barrier discharge plasma. *Nanomaterials* **2019**, *9*, 720. [[CrossRef](#)] [[PubMed](#)]
233. Oda, T.; Kato, T.; Takahashi, T.; Shimizu, K. Nitric oxide decomposition in air by using nonthermal plasma processing with additives and catalyst. *IEEE Trans. Ind. Appl.* **1998**, *34*, 268–272. [[CrossRef](#)]
234. Baeva, M.; Gier, H.; Pott, A.; Uhlenbusch, J.; H02schele, J.; Steinwandel, J. Erratum: “Studies on Gas Purification by a Pulsed Microwave Discharge at 2.46 GHz in Mixtures of N₂/NO/O₂ at Atmospheric Pressure” [Plasma Chemistry and Plasma Processing, Vol. 21, No. 2, 2001]. *Plasma Chem. Plasma Process.* **2002**, *22*, 197. [[CrossRef](#)]
235. Baeva, M.; Gier, H.; Pott, A.; Uhlenbusch, J.; Höschele, J.; Steinwandel, J. Pulsed microwave discharge at atmospheric pressure for NO_x decomposition. *Plasma Sources Sci. Technol.* **2002**, *11*, 1–9. [[CrossRef](#)]
236. Hueso, J.L.; Gonzalez-Elipse, A.R.; Cotrino, J.; Caballero, A. Plasma chemistry of NO in complex gas mixtures excited with a surfatron launcher. *J. Phys. Chem. A* **2005**, *109*, 4930–4938. [[CrossRef](#)]
237. Hueso, J.L.; González-Elipse, A.R.; Cotrino, J.; Caballero, A. Removal of NO in NO/N₂, NO/N₂/O₂, NO/CH₄/N₂, and NO/CH₄/O₂/N₂ Systems by Flowing Microwave Discharges. *J. Phys. Chem. A* **2007**, *111*, 1057–1065. [[CrossRef](#)]
238. Schütz, A.; Lara-Ortega, F.J.; Klute, F.D.; Brandt, S.; Schilling, M.; Michels, A.; Veza, D.; Horvatic, V.; García-Reyes, J.F.; Franzke, J. Soft Argon-Propane Dielectric Barrier Discharge Ionization. *Anal. Chem.* **2018**, *90*, 3537–3542. [[CrossRef](#)]
239. Brandt, S.; Klute, F.D.; Schütz, A.; Franzke, J. Dielectric barrier discharges applied for soft ionization and their mechanism. *Anal. Chim. Acta* **2017**, *951*, 16–31. [[CrossRef](#)]
240. Zuliang, W.U.; Hou, P.; Zhao, J.; Wang, J.; Yan, X.U.; Yao, S. Experimental Study of Simultaneous Desulfurization and Denitrification by Corona Discharge Coupling Wet Absorption. *High. Volt. Eng.* **2016**, *42*, 398–404.
241. Chen, S.; Wang, T.; Wang, H.; Wu, Z. Insights into the reaction pathways and mechanism of NO removal by SDBD plasma via FT-IR measurements. *Fuel Process. Technol.* **2019**, *186*, 125–136. [[CrossRef](#)]
242. Zhang, Q.Z.; Bogaerts, A. Propagation of a plasma streamer in catalyst pores. *Plasma Sources Sci. Technol.* **2018**, *27*, 035009. [[CrossRef](#)]
243. Hong, L.; Chen, D.; Yang, M.; Yin, L.; Wang, D.; Wang, L. Interaction between NO and SO₂ removal processes in a pulsed corona discharge plasma (PCDP) reactor and the mechanism. *Chem. Eng. J.* **2019**, *359*, 1130–1138. [[CrossRef](#)]
244. Zhang, H.; Li, K.; Li, L.; Liu, L.; Meng, X.; Sun, T.; Jia, J.; Fan, M. High efficient styrene mineralization through novel NiO-TiO₂-Al₂O₃ packed pre-treatment/treatment/post-treatment dielectric barrier discharge plasma. *Chem. Eng. J.* **2018**, *343*, 759–769. [[CrossRef](#)]
245. Huang, H.; Ye, D.; Huang, B.; Wei, Z. Vanadium Supported on Viscose-Based Activated Carbon Fibers Modified By Oxygen Plasma For The Scr Of No. *Catal. Today* **2008**, *139*, 100–108. [[CrossRef](#)]
246. Liu, L.; Zheng, C.; Wu, S.; Gao, X.; Ni, M.; Cen, K. Manganese-cerium oxide catalysts prepared by non-thermal plasma for NO oxidation: Effect of O₂ in discharge atmosphere. *Appl. Surf. Sci.* **2017**, *416*, 78–85. [[CrossRef](#)]
247. An, J.; Jiang, Y.; Zhang, Z.; Ma, X.; Wang, T.; Shang, K.; Li, J. Oxidation characteristics of mixed NO and Hg₀ in coal-fired flue gas using active species injection generated by surface discharge plasma. *Chem. Eng. J.* **2016**, *288*, 298–304. [[CrossRef](#)]
248. Cui, S.; Hao, R.; Fu, D. Integrated method of non-thermal plasma combined with catalytical oxidation for simultaneous removal of SO₂ and NO. *Fuel* **2019**, *246*, 365–374. [[CrossRef](#)]
249. Zhao, D.; Yu, F.; Zhou, A.; Ma, C.; Dai, B. High-efficiency removal of NO_x using dielectric barrier discharge nonthermal plasma with water as an outer electrode. *Plasma Sci. Technol.* **2018**, *20*, 014020. [[CrossRef](#)]

250. Peng, M.; Zhao, R.; Xia, M.; Li, C.; Gong, X.; Wang, D.; Xia, D. Study on the mechanism of NO removal by plasma-adsorption catalytic process. *Fuel* **2017**, *200*, 290–298. [[CrossRef](#)]
251. Park, H.W.; Choi, S.; Park, D.W. Simultaneous treatment of NO and SO₂ with aqueous NaClO₂ solution in a wet scrubber combined with a plasma electrostatic precipitator. *J. Hazard. Mater.* **2015**, *285*, 117–126. [[CrossRef](#)] [[PubMed](#)]
252. Wang, T.; Liu, H.; Zhang, X.; Liu, J.; Zhang, Y.; Guo, Y.; Sun, B. Catalytic conversion of NO assisted by plasma over Mn-Ce/ZSM5-multi-walled carbon nanotubes composites: Investigation of acidity, activity and stability of catalyst in the synergic system. *Appl. Surf. Sci.* **2018**, *457*, 187–199. [[CrossRef](#)]
253. Li, H.; Jiang, X.; Zheng, X. Plasma-assisted CuO/CeO₂/TiO₂-γ-Al₂O₃ catalysts for NO+CH₄ reaction and NO temperature programmed desorption studies. *Appl. Surf. Sci.* **2013**, *280*, 273–281. [[CrossRef](#)]
254. Dang, X.; Qin, C.; Huang, J.; Teng, J.; Huang, X. Adsorbed benzene/toluene oxidation using plasma driven catalysis with gas circulation: Elimination of the byproducts. *J. Ind. Eng. Chem.* **2016**, *37*, 366–371. [[CrossRef](#)]
255. Tang, X.; Gao, F.; Xiang, Y.; Yi, H.; Zhao, S. Low temperature catalytic oxidation of nitric oxide over the Mn-CoOx catalyst modified by nonthermal plasma. *Catal. Commun.* **2015**, *64*, 12–17. [[CrossRef](#)]
256. Niu, J.; Yang, X.; Zhu, A.; Shi, L.; Sun, Q.; Xu, Y.; Shi, C. Plasma-assisted selective catalytic reduction of NO_x by C₂H₂ over Co-HZSM-5 catalyst. *Catal. Commun.* **2006**, *7*, 297–301. [[CrossRef](#)]
257. Broer, S.; Hammer, T. Selective catalytic reduction of nitrogen oxides by combining a non-thermal plasma and a V₂O₅-WO₃/TiO₂ catalyst. *Appl. Catal. B: Environ.* **2000**, *28*, 101–111. [[CrossRef](#)]
258. Fan, H.Y.; Shi, C.; Li, X.S.; Yang, X.F.; Xu, Y.; Zhu, A.M. Low-temperature NO_x Selective Reduction by Hydrocarbons on H-Mordenite Catalysts in Dielectric Barrier Discharge Plasma. *Plasma Chem. Plasma Process.* **2009**, *29*, 43–53. [[CrossRef](#)]
259. Li, K.; Tang, X.; Yi, H.; Ning, P.; Song, J.; Wang, J. Mechanism of Catalytic Oxidation of NO over Mn-Co-Ce-Ox Catalysts with the Aid of Nonthermal Plasma at Low Temperature. *Ind. Eng. Chem. Res.* **2011**, *50*, 11023–11028. [[CrossRef](#)]
260. Cho, B.K.; Lee, J.H.; Crellin, C.C.; Olson, K.L.; Hilden, D.L.; Kim, M.K.; Kim, P.S.; Heo, I.; Oh, S.H.; Nam, I.S. Selective catalytic reduction of NO_x by diesel fuel: Plasma-assisted HC/SCR system. *Catal. Today* **2012**, *191*, 20–24. [[CrossRef](#)]
261. Pan, H.; Su, Q.; Wei, J.; Jian, Y. Promotion of Nonthermal Plasma on the SO₂ and H₂O Tolerance of Co-In/Zelolites for the Catalytic Reduction of NO_x by C₃H₈ at Low Temperature. *Plasma Chem. Plasma Process.* **2015**, *35*, 831–844. [[CrossRef](#)]
262. Wang, T.; Zhang, X.; Liu, J.; Liu, H.; Wang, Y.; Sun, B. Effects of temperature on NO_x removal with Mn-Cu/ZSM5 catalysts assisted by plasma. *Appl. Therm. Eng.* **2018**, *130*, 1224–1232. [[CrossRef](#)]
263. Tao, W.; Liu, H.; Zhang, X.; Guo, Y.; Zhang, Y.; Yang, W.; Sun, B. A plasma-assisted catalytic system for NO removal over CuCe/ZSM-5 catalysts at ambient temperature. *Fuel Process. Technol.* **2017**, *158*, 199–205.
264. Jögi, I.; Stamate, E.; Irimiea, C.; Schmidt, M.; Brandenburg, R.; Hołub, M.; Bonisławski, M.; Jakubowski, T.; Kääriäinen, M.-L.; Cameron, D.C. Comparison of direct and indirect plasma oxidation of NO combined with oxidation by catalyst. *Fuel* **2015**, *144*, 137–144.
265. Li, K.; Tang, X.; Yi, H.; Ning, P.; Xiang, Y.; Wang, J.; Wang, C.; Peng, X. Research on manganese oxide catalysts surface pretreated with non-thermal plasma for NO catalytic oxidation capacity enhancement. *Appl. Surf. Sci.* **2013**, *264*, 557–562. [[CrossRef](#)]
266. Garraud, O.; Coppo, P. Types of fresh plasma with focus on therapeutic plasma exchange. *Transfus. Apher. Sci.* **2019**, *58*, 258–261. [[CrossRef](#)] [[PubMed](#)]
267. Ibrahimoglu, B.; Yilmazoglu, M.Z. Numerical modeling of a downdraft plasma coal gasifier with plasma reactions. *Int. J. Hydrog. Energy* **2019**, *67*, 165–173. [[CrossRef](#)]

